Naval Surface Warfare Center
Carderock Division
West Bethesda, MD 20817-5700

NAVSEA
WARFARE CENTERS
Carderock Division

NSWCCD-50-TR–2012/040 December 2012
Hydromechanics Department Report

Validation of Numerical Predictions of the Impact Forces and Hydrodynamics of a Deep-V Planing Hull

By
Thomas T. O'Shea, Kyle A. Brucker, Donald Wyatt, Douglas G. Dommermuth, Jonathan Ward, Sheguang Zhang, Kenneth Weems, Woei-Min Lin, Carolyn Judge, Allen Engle, Thomas C. Fu, and Anne M. Fullerton

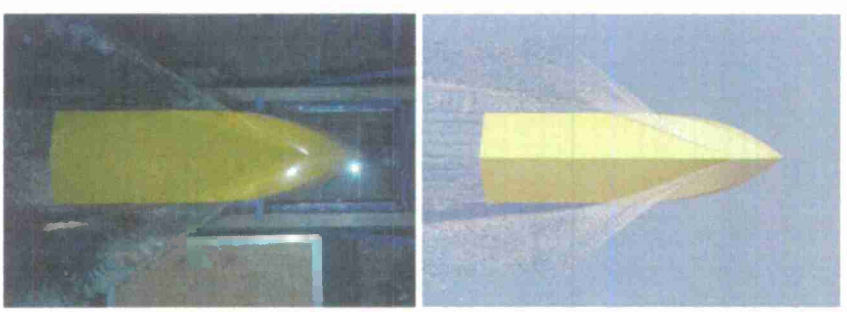

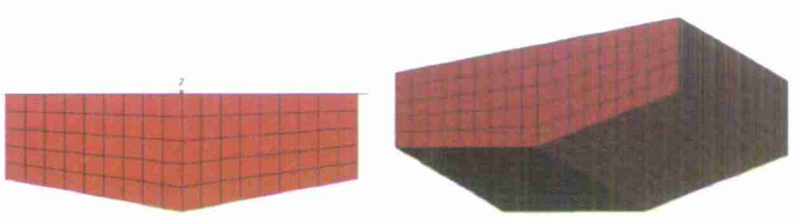

REPORT DOCUMENTATION PAGE

Form Approved
OMB No. 0704-0188

1. REPORT DATE *(DD-MM-YYYY)*	2. REPORT TYPE	3. DATES COVERED *(From - To)*
December 2012	Final	January 2011-December 2012

4. TITLE AND SUBTITLE
Validation of Numerical Predictions of the Impact Forces and Hydrodynamics of a Deep-V Planing Hull

5a. CONTRACT NUMBER
N00167-10-D-0004

5b. GRANT NUMBER

5c. PROGRAM ELEMENT NUMBER

6. AUTHOR(S)
Thomas T. O'Shea, Kyle A. Brucker, Donald Wyatt, Douglas G. Dommermuth, Jonathan Ward, Sheguang Zhang, Kenneth Weems, Woei-Min Lin, Carolyn Judge, Allen Engle, Thomas C. Fu, and Anne M. Fullerton

5d. PROJECT NUMBER

5e. TASK NUMBER
0007

5f. WORK UNIT NUMBER
11-1-6540-448-20

7. PERFORMING ORGANIZATION NAME(S) AND ADDRESS(ES) AND ADDRESS(ES)

Naval Surface Warfare Center
Carderock Division
9500 Macarthur Boulevard
West Bethesda, MD 20817-5700

8. PERFORMING ORGANIZATION REPORT NUMBER

NSWCCD-50-TR-2012/040

9. SPONSORING / MONITORING AGENCY NAME(S) AND ADDRESS(ES)
Robert Brizzolara
Office of Naval Research
845 N. Randolph Street
Building 875
Arlington, VA 22203

10. SPONSOR/MONITOR'S ACRONYM(S)
ONR

11. SPONSOR/MONITOR'S REPORT NUMBER(S)

12. DISTRIBUTION / AVAILABILITY STATEMENT Approved for public release; distribution unlimited.

13. SUPPLEMENTARY NOTES

14. ABSTRACT

Over the past few years much progress has been made in Computational Fluid Dynamics (CFD) in its ability to accurately simulate the hydrodynamics associated with a deep-V monohull planing craft. This work has focused on not only predicting the hydrodynamic forces and moments, but also the complex multiphase free-surface flow field generated by a deep-V monohull planing boat at high Froude numbers. One of these state of the art CFD codes is Numerical Flow Analysis (NFA). NFA provides turnkey capabilities to model breaking waves around a ship, including both plunging and spilling breaking waves, the formation of spray, and the entrainment of air. NFA uses a Cartesian-grid formulation with immersed body and volume-of-fluid methods. Another available code is the Large Amplitude Motion Program (LAMP), which is a nonlinear time-domain ship motions and loads program.

15. SUBJECT TERMS

16. SECURITY CLASSIFICATION OF:			17. LIMITATION OF ABSTRACT	18. NO. OF PAGES	19a. RESPONSIBLE PERSON
a. REPORT	b. ABSTRACT	c. THIS PAGE		54+viii	Anne Fullerton
UNCLASSIFIED	UNCLASSIFIED	UNCLASSIFIED			19b. TELEPHONE NUMBER 301-227-5887

14. ABSTRACT (continued)

The focus of this paper is to describe and document a recent effort to assess these numerical codes for the prediction of deep-V planing craft hydrodynamic forces and moments and evaluate how well NFA models the complex multiphase flows associated with high Froude number flows, specifically the formation of the spray sheet. This detailed validation effort was composed of three parts. The first part focused on assessing the codes' ability to predict pressures on the surface of a 10 degree deadrise wedge during impact with an undisturbed free surface. Detailed comparisons of NFA to pressure gauges show that NFA accurately predicted pressures during the slamming event. Comparisons of experimental measurements with LAMP predictions showed fairly good agreement, though LAMP tends to overpredict pressures.

The second part examines the codes' ability to match sinkage, trim and resistance from Fridsma's experiments performed on constant deadrise planing hulls. Results show good agreement between NFA and experimentally measured values, as well as values calculated using Savitsky's parametric equations. Fairly good agreement was shown between LAMP and experimental values as well, with trim predictions matching well and heave tending to be over-predicted.

The final part of the validation study focused on assessing how the codes' ability to accurately model the complex multiphase flow associated with high Froude number flows, specifically the formation of the spray sheet. Comparisons to underwater photographs illustrate NFA's ability to model the formation of the spray sheet and the free surface turbulence associated with planing boat hydrodynamics. Though LAMP was not used to model the complex flow, it accurately predicted the model heave and trim. Overall these three validation studies provide a detailed assessment on the current capabilities of NFA and LAMP to predict the hydrodynamics of a deep-V planing hull.

CONTENTS

FIGURES

TABLES

INTERNATIONAL SYSTEM OF UNITS (SI) CONVERSION LIST

U.S. CUSTOMARY	METRIC EQUIVALENT
1 inch (in)	25.4 millimeter (mm), 0.0254 meter (m)
1 foot (ft)	0.3048 meter (m)
1 pound-mass (lbm)	0.4536 kilograms (kg)
1 pound-force (lbf)	4.448 Newtons (N)
1 foot-pound-force (ft-lbf)	1.3558 Newton-meters (N-m)
1 foot per second (ft/s)	0.3048 meter per second (m/s)
1 knot (kt)	1.6878 feet per second (ft/s) 0.5144 meter per second (m/s)
1 horsepower (hp)	0.7457 kilowatts (kW)
1 long ton (LT)	1.016 tonnes 1.016 metric tons 1016 kilograms (kg) 2240 pounds
1 inch water (60F)	248.8 Pascals (Pa)

This page intentionally left blank.

ABSTRACT

Over the past few years much progress has been made in Computational Fluid Dynamics (CFD) in its ability to accurately simulate the hydrodynamics associated with a deep-V monohull planing craft. This work has focused on not only predicting the hydrodynamic forces and moments, but also the complex multiphase free-surface flow field generated by a deep-V monohull planing boat at high Froude numbers. One of these state of the art CFD codes is Numerical Flow Analysis (NFA). NFA provides turnkey capabilities to model breaking waves around a ship, including both plunging and spilling breaking waves, the formation of spray, and the entrainment of air. NFA uses a Cartesian-grid formulation with immersed body and volume-of-fluid methods. Another available code is the Large Amplitude Motion Program (LAMP), which is a nonlinear time-domain ship motions and loads program.

The focus of this report is to describe and document a recent effort to assess these numerical codes for the prediction of deep-V planing craft hydrodynamic forces and moments and evaluate how well NFA models the complex multiphase flows associated with high Froude number flows, specifically the formation of the spray sheet. This detailed validation effort was composed of three parts. The first part focused on assessing the codes' ability to predict pressures on the surface of a 10 degree deadrise wedge during impact with an undisturbed free surface. Detailed comparisons of NFA to pressure gauges show that NFA accurately predicted pressures during the slamming event. Comparisons of experimental measurements with LAMP predictions showed fairly good agreement, though LAMP tends to over-predict pressures.

The second part examines the codes' ability to match sinkage, trim and resistance from Fridsma's experiments performed on constant deadrise planing hulls. Results show good agreement between NFA and experimentally measured values, as well as values calculated using Savitsky's parametric equations. Fairly good agreement was shown between LAMP and experimental values as well, with trim predictions matching well and heave tending to be over-predicted.

The final part of the validation study focused on assessing how the codes' ability to accurately model the complex multiphase flow associated with high Froude number flows, specifically the formation of the spray sheet. Comparisons to underwater photographs illustrate NFA's ability to model the formation of the spray sheet and the free surface turbulence associated with planing boat hydrodynamics. Though LAMP was not used to model the complex flow, it accurately predicted the model heave and trim. Overall these three validation studies provide a detailed assessment on the current capabilities of NFA and LAMP to predict the hydrodynamics of a deep-V planing hull.

ACKNOWLEDGEMENTS

This work is supported by the Office of Naval Research (ONR), program manager Bob Brizzolara. The NFA numerical simulations have been performed on the Cray XE6 platforms located at the U.S. Army Engineering Research and Development Center (ERDC) and the Air Force Research Laboratory (AFRL). NFA research and development has been sponsored over the years by Dr. Steve Russell and Dr. L. Patrick Purtell. SAIC IR&D also supported the development of NFA. The NFA work is also supported in part by a grant of computer time from the Dept. of Defense High Performance Computing Modernization Program, http://www.hpcmo.hpc.mil/. Animations of NFA simulations are available at http://www.youtube.com/waveanimations.

ADMINISTRATIVE INFORMATION

The work described in this report was performed by the Science and Technology Branch of the Resistance and Propulsion Division (Code 583) of the Hydromechanics Department at the Naval Surface Warfare Center, Carderock Division (NSWCCD). The work was performed under work request N00167-10-D-0004, and work unit number 11-1-6540-448-20.

INTRODUCTION

As interest in high-speed craft has grown in recent years, the number of efforts to experimentally characterize and numerically simulate their behavior has also increased. Due to the low draft of high-speed planing craft, small motions can result in large changes in wetted surface area, and linearity assumptions are less valid since hydrodynamic forces dominate in the planing regime, making these problems especially challenging. Building upon the classic prismatic planing hull experimental efforts of Fridsma [1] and Savistsky [2], a number of researchers have focused on the problem of dynamic stability of high speed planing craft. Codega and Lewis [3] described a class of high-speed planing boats that exhibited dynamic instabilities such as the craft trimming by the bow, rolling to a large angle of heel to port, and broaching violently to starboard. Blount and Codega [4] presented data on boats that exhibited non-oscillatory dynamic instabilities and suggested quantitative criteria for development of dynamically stable planing boats. Katayama et al. [5] found that instability is strongly influenced by the running attitude of the hull at high speeds. Troesch [6], and Troesch & Falzarano [7] have investigated the dynamic behavior of planing, and porpoising behavior. Research done at the Stevens Institute of Technology has investigated the transverse stability of planing craft using coupled linear sway/roll/yaw equations of motion [8].

Significant progress has been made in Computational Fluid Dynamics (CFD) and its ability to accurately simulate the hydrodynamics associated with a deep-V monohull planing craft (see [9], [10], [11], [12]). The validation effort described in this report is focused on predicting the hydrodynamic forces and moments, but also the complex multiphase free-surface flow field generated by a deep-V monohull planing boat at high Froude numbers. One of these state of the art CFD codes is Numerical Flow Analysis (NFA). NFA provides turnkey capabilities to model breaking waves around a ship, including both plunging and spilling breaking waves, the formation of spray, and the entrainment of air. NFA uses a Cartesian-grid formulation with immersed body and volume-of-fluid (VOF) methods. O'Shea et al [13] describes the code and recent applications to naval problems. Another available code is the Large Amplitude Motion Program (LAMP), which is a nonlinear time-domain ship motions and loads program.

This report describes a recent effort to assess NFA and LAMP for the prediction of deep-V planing craft hydrodynamic forces and moments and evaluate how well they model the complex multiphase flows associated with high Froude number flows, specifically the formation of the spray sheet. This detailed validation effort is composed of three parts. The first part focuses on assessing the codes' ability to predict pressures on the surface of a 10 degree deadrise wedge during impact with an undisturbed free surface. The second part examines the codes' ability to match sinkage, trim and resistance from experiments performed on constant deadrise planing hulls, detailed in Fridsma [1]. The final part of the validation study is focused on assessing the ability of NFA to accurately model the complex multiphase flow associated with high Froude number flows, specifically the formation of the spray sheet. Additionally, LAMP predictions were performed to compare with the trim and heave values of this third experiment.

NUMERICAL APPROACH-NFA

NFA utilizes the Navier-Stokes equations in a cut-cell, Cartesian-grid formulation with interface-capturing to model the unsteady flow of air and water around moving bodies. The interface-capturing of the free surface uses a second-order accurate, volume-of-fluid technique. NFA uses an implicit subgrid-scale model that is built into the treatment of the convective terms in the momentum equations [14]. A panelized surface representation of the ship hull (body) is all that is required as input in terms of body geometry. Domain decomposition is used to distribute portions of the grid over a large number of processors. The algorithm is implemented on parallel computers using FORTRAN 2003 and the Message Passing Interface (MPI). The interested reader is referred to [13], [15], and [16], for a detailed description of the numerical algorithm and of its implementation on distributed memory high performance computing (HPC) platforms.

NUMERICAL APPROACH-LAMP

The Large Amplitude Motion Program (LAMP) is a nonlinear time-domain ship motions and loads program. In addition to the ship motions calculated by LAMP, four different methods in LMPOUND are used for impact load calculations in this task, as shown in Figure 1. They are:

- Wedge approximation: sectional impact forces are calculated from the momentum of a wedge approximation for the port and starboard sides of the hull, and pressures are determined by distributing this force evenly over the wetted half-beam
- Richard Lewis's effective pressure method: formulas derived from momentum theory for a constant velocity wedge impact are used to calculate the vertical force and effective pressure
- 2D Wagner's formula: wedge approximation is used to obtain the transverse pressure distribution and the impact force, all in closed analytical forms.
- SLAM2D: impact force and pressure are computed using SLAM2D program, a 2D potential flow (infinite frequency) panel code developed by Zhao and Faltinsen [17].

Further descriptions of these four methods are provided in the following section. An impact load calculation based on a conformal mapping solution is also available in LMPOUND, but is not discussed in this report. The integration of impact pressure into the pressure interface code LMPRES is also being performed under the present task but is not discussed in this report.

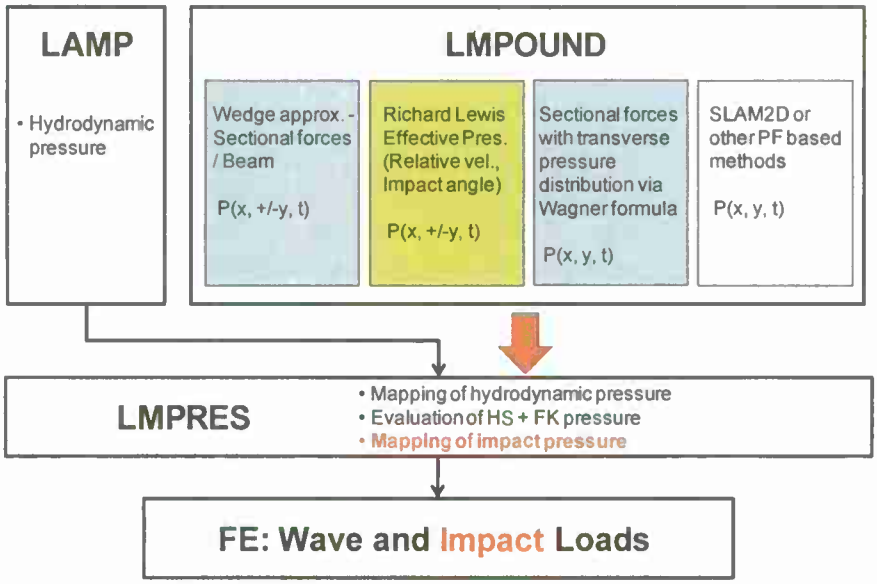

Figure 1: Impact load and pressure calculation methods in LMPOUND.

Wedge Approximation

In this method, slamming forces on a ship are solved using a simplified 2D wedge impact model for a ship hull modeled as a set of 2D sections. The sectional force per unit length is equal to the time rate of change of the section's momentum:

$$F = \frac{d(MV)}{dt} \tag{1}$$

$$= M\frac{dV}{dt} + V\frac{dM}{dt}$$

where M=added mass of a 2D wedge
V=velocity
t=time

The first term on the right-hand side, the mass multiplied by acceleration, is an inertia term and is ignored in the slamming force calculations, i.e. the slamming force is modeled as a wedge impact with a constant velocity. The added mass of a 2D wedge is calculated based on Wagner's theory [18]:

$$M = \frac{\pi}{2}\rho C_m((b/2)\psi)^2 \tag{2}$$

where ρ= water density
C_m=added mass coefficient, explained below
b=beam
and ψ=increase in beam, explained below

The deadrise angle and half-beam are computed at each step based on the relative submergence of the ship section, which is calculated from the ship's rigid body motion and the incident wave elevation. Similarly, the impact velocity is computed from the velocity of the section's keel point relative to the incident wave surface. The added mass coefficient is represented by:

$$C_m = \left(1 - \frac{\beta}{2\pi}\right)^2 \tag{3}$$

where β=deadrise angle

and ψ represents an increase in beam based on Pierson's Hypothesis [19] which is a linear interpolation of Wagner's splash-up factor at 0° deadrise angle and Von Karman's (1929) splash-up factor (no splash-up) at 90° deadrise angle:

$$\psi = \frac{\pi}{2} - \beta\left(1 - \frac{2}{\pi}\right) \tag{4}$$

This term is also referred to as "splash-up" and is used to account for the jet of water formed near the intersection of the body and the free surface. The added mass is finite-differenced in time with finer time step size than with the LAMP calculation to help resolve the impact event. To ensure the accuracy of the time derivative calculation of the added mass, the deadrise angle is smoothed between the panels that make up the section cut.

An average pressure on the section can be taken to be the sectional vertical force divided across the wetted beam:

$$p = \frac{F}{b\psi} \tag{5}$$

In the LMPOUND implementation, two wedge impact problems are solved for each section: one for the port side and one for the starboard side, so that differences in deadrise angles due to an oblique incident wave and the ship's roll can be taken into account. The average pressure for each half-wedge is calculated separately as well.

Richard Lewis Effective Pressure

In the 1995 report by Richard Lewis [20], an expression for the "effective engineering impact pressure" as a function of deadrise angle and relative vertical velocity between the wedge and free surface is given as:

$$p_{eff} = \rho V^2 \cos(\beta)\sqrt{\frac{25 + \tan^2(\beta)}{9\tan^2(\beta)}} \tag{6}$$

where ρ is the mass density of the fluid, V is the relative vertical velocity between the wedge and free surface, and β is the deadrise angle or relative angle between the free surface and the wedge section at the free surface intersection. For the LMPOUND implementation, the free surface slope above the keel is used along with the deadrise angle of the panel intersecting the free

surface to compute β. V, the velocity, is taken as the sum of the downward velocity of the wedge and the upward velocity of the free surface at the point above the keel.

This equation is based on the vertical force required to displace the volume of water by the wedge into the splash-up region and is obtained by using momentum theory. The force is then divided over the beam of the splash-up region. "Effective engineering pressure" refers to the fact that it is an average pressure across the wedge and does not represent the actual pressure at a particular location on the wedge, such as the peak, but a pressure that should be applied to structural panels. For the development of time domain pressure distributions, it will be necessary to correlate the position and size of the structural panels with the splash-up region.

Wagner Formulation

Wagner's water impact pressure and force formulations are obtained by solving a 2D wedge entry problem using potential flow theory.

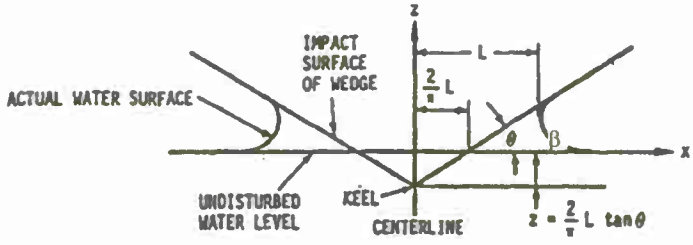

Figure 2: Schematic of a 2D wedge entry problem [21].

In Figure 2, the wedge is entering calm water with the downward speed, V, deadrise angle, β, and the instantaneous wetted beam, L, which includes the free surface splash-up. The splash-up is described by an empirical factor, ψ, which has different values based on different approaches/assumptions. For example, in Wagner's form, $\psi=\pi/2$, and in Pierson's form, $\psi= \pi/2 - \beta(1-2/\pi)$, as explained above. Figure 2 illustrates the Wagner form with $\psi=\pi/2$. The velocity potential, φ, for this problem can be solved analytically by imposing the boundary conditions on the wetted beam such that $\partial\varphi/\partial n=V$, and on the free surface $\varphi=0$. The impact pressure on the wetted length, L, can be obtained using Bernoulli's equation,

$$p(X) = \frac{1}{2}\rho V^2\left[\frac{2\psi}{tan\beta\sqrt{1-X^2}} - \frac{X^2}{1-X^2}\right] + \rho L\frac{dV}{dt}\sqrt{1-X^2} \qquad (7)$$

where X is the non-dimensionalized horizontal coordinate, x, with respect to the wetted length, L, i.e. $X=x/L$.

In Wagner's pressure formulation, there are three terms. The first term is associated with the time rate of the added mass approximated by an expanding flat plate. This term is the primary contributor to the impact pressure. The second term is associated with the quadratic term in the Bernoulli's equation. This term becomes important near the edge of the wetted surface where the fluid velocity changes rapidly. The last term is the pressure due to the accelerating added mass. If the duration of the impact is sufficiently short and the change in the impact velocity V is

negligible, this term is insignificant and can be ignored. Figure 3 shows pressure distributions based on Wagner's formula for a 10° and a 30° wedge. Figure 3 shows that the impact pressure increases rapidly towards the edge of the wetted surface for the 10° wedge; while for the 30° wedge, the pressure is distributed more evenly across the wetted length.

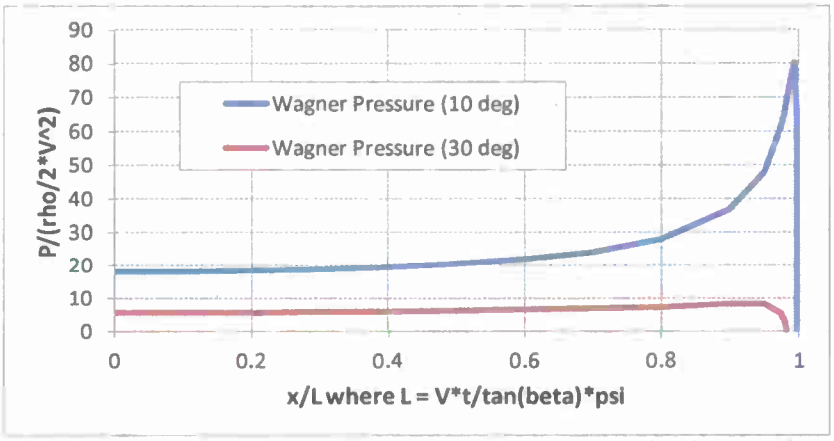

Figure 3: Wagner's pressure distribution on the wetted length of 10° and 30° wedges.

Integrating Wagner's pressure along the wetted length, L, yields Wagner's impact force. Note that Wagner's pressure is singular and goes to negative ∞ at $X(=x/L)=1$ due to the deficiency in potential flow formulation, so the pressure integration should be carried out from $X=0$ to $X=X_0$ where X_0 is the zero of the pressure equation, i.e. $P(X_0)=0$,

$$X_0 = \sqrt{\frac{-a+\sqrt{a^2+4a}}{2}}, \qquad a = \frac{4\psi^2}{\tan^2\beta} \tag{8}$$

The Wagner's impact force formula is given by:

$$F = \frac{1}{2}\rho V^2 L\left[\frac{2\psi}{\tan\beta}\sin^{-1}(X_0) + X_0 - \frac{1}{2}\ln\left(\frac{1+X_0}{1-X_0}\right)\right] + \frac{1}{2}\rho L^2\frac{dV}{dt}\left[\sqrt{1-X_0^2} - 1 + \sin^{-1}(X_0)\right] \tag{9}$$

The terms in the first square bracket are from the integration of the first two terms in the pressure formula, and are therefore important. The second square bracket can be ignored when the acceleration during impact is negligible. Figure 4 shows the normalized vertical impact force on the wedge as a function of deadrise angle.

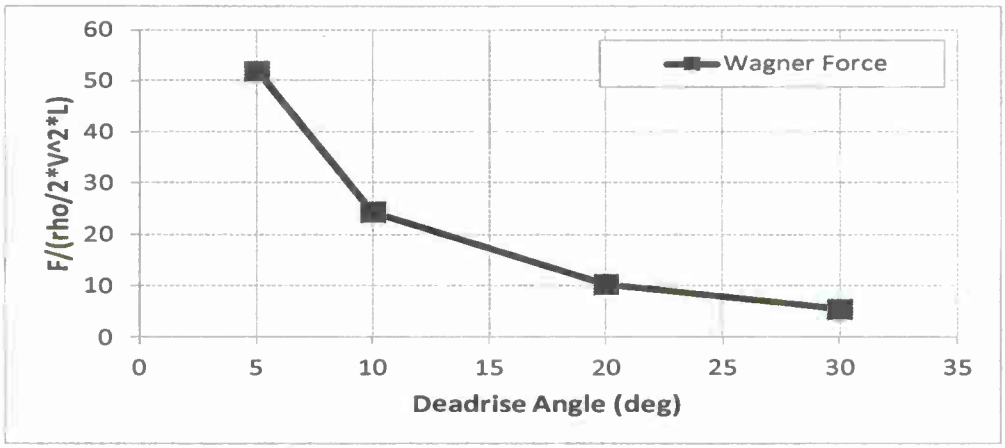

Figure 4: Wagner's impact force vs. deadrise angles.

There are pros and cons of using Wagner's formulation for water impact problems:
The pros include:

- Both Wagner's pressure and force formulations are analytical and of closed form. Therefore, they are accurate in their own valid domains.
- The formula is robust, easy to use and implement, and fast to calculate.
- The formula can be a good approximation to more general wedge-like sections.
- The formula can include the acceleration effect.

The cons include:

- Inaccurate when deadrise angle is too small, e.g. $\beta<5°$.
- Not applicable in its current form for oblique impact or non-wedge type sections.
- May over-predict the impact pressures in comparison to experiments.

The numerical implementations of Wagner's pressure and force formulations in LMPOUND are straightforward. They include:

- At a given time instant and on each side of the wedge, compute the deadrise angle, β, and the wetted half beam length, *b/2*, at the intersection between the wedge edge and the free surface (i.e. the wetted beam length without the splash-up effect).
- Calculate the instantaneous wetted length, L, which includes the splash-up.
- Compute X_0 to determine the effective wetted length between 0 and X_0 on which $p(X)\geq 0$.
- Preselect collocation points between $[0, X_0]$ for pressure calculation.
- Compute the impact pressures on the collocation points between $[0, X_0]$.
- Compute the impact force acting on the same side of the wedge.
- Repeat the pressure and force calculation on the other side of the wedge.
- Output the impact pressure together with the lateral and vertical locations of the collocation points on each side of the wedge; add the impact force on two sides of the wedge and output the total impact force on the whole wedge.
- Repeat the above procedures the each time step of the impact event.

SLAM2D Method

SLAM2D was developed by Marintek in Norway. The version (v2.0) used in LAMP was developed and delivered to SAIC under the Navy DASS (Dynamic Assessment of Surface Ship)

project in 1998. SLAM2D has two solution methods: (1) generalized Wagner approach, and (2) fully nonlinear approach. The generalized Wagner approach is discussed in this section and illustrated in Figure 5 and Figure 6.

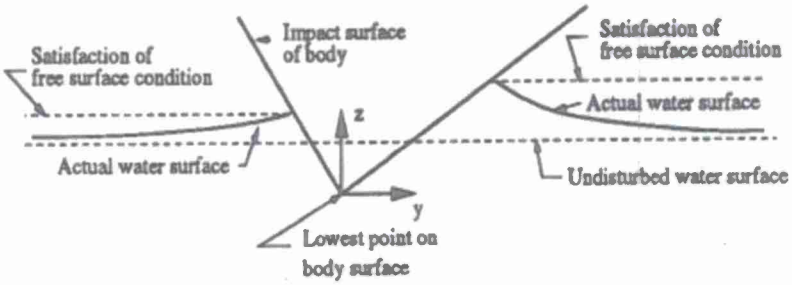

Figure 5: Sketch of 2D wedge impact.

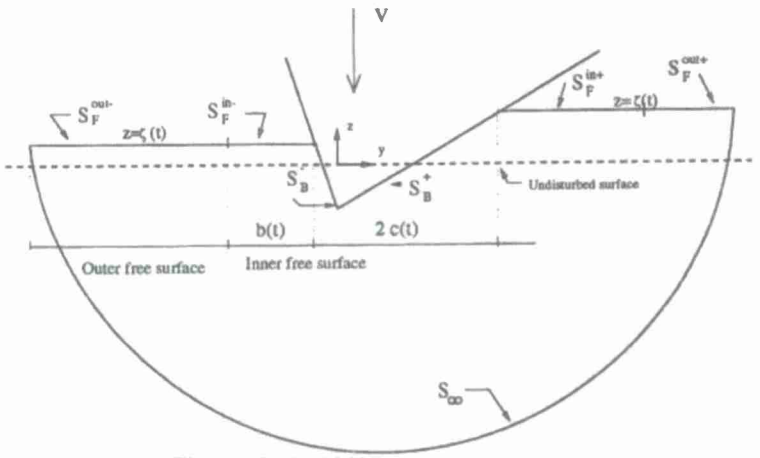

Figure 6: SLAM2D solution domain.

At a given time instant during impact, SLAM2D solves a potential flow boundary value problem for a wedge-entry. Unlike the classical Wagner approach that involves an expanding flat plate with splash up, SLAM2D adopted a more generalized approach in a sense that:

- The boundary value problem is solved with respect to the actual 2D cross section, meaning that the boundary conditions are applied on the actual body surface and elevated free surface due to splash up.
- Splash-up is computed numerically with a local jet flow solution near the intersections between the body and the free surface.
- Oblique impact can be considered, including the effects due to not only the vertical but horizontal and rotational velocities of the 2D section.

However, there are certain limitations in the SLAM2D version v2.0 including:

- Certain 2D shapes, including all shapes not monotonically expanding from the keel, are not allowed, forcing many real ship sections, such as bulbous bow sections, to be approximated.
- Time consuming (40 times slower than the direct Wagner formula calculation).
- Not accurate or valid during the initial impact phase when the submergence is less than 10% of the draft.

- Issues in numerical implementation – In some applications, the simulation is not as robust as others, pointing to some numerical implementation issues.

Nevertheless, SLAM2D is still a valuable tool to be used either as a validation tool for other water impact models or as a direct simulation tool for water impact problems.

Planing Boat Approach

When a small boat travels at high speed (roughly at a Froude Number greater than 0.7), it typically operates in a planing mode. At these speeds, LAMP's standard "low-speed" wave-body hydrodynamics model, which uses a 3-D potential flow panel method to compute a disturbance pressure over the hull surface, is no longer applicable, so a planing boat hydrodynamic model based on a 2½-dimension (2.5-D) theory is used. In this model, the vessel is represented by a set of cross-sections distributed along the boat length and a 2-D hydrodynamic impact problem is solved in each plane based on the analytical solution for a wedge impact and the instantaneous relative motion of the boat. The sectional forces are integrated along the ship length and added to the normal 3-D body-nonlinear hydrostatic restoring and Froude-Krylov pressure forces, as well as any external forces models (rudders, roll damping, etc.) to get the total forces acting on the boat at each time step.

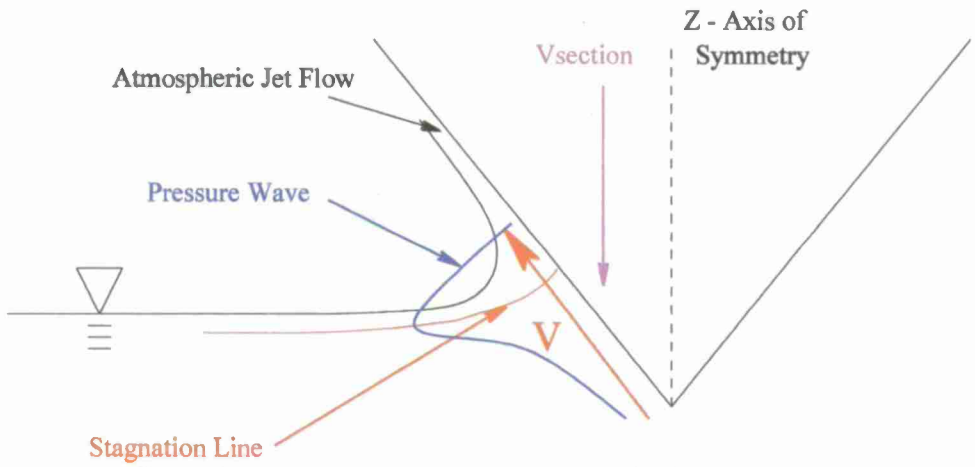

Figure 7. Local Jet Flow Hydrodynamics of the Wedge Impact.

In the planing force model, the slender body approximation is used to reduce the steady 3-D free surface hydrodynamic in calm water problem to a 2-D unsteady problem in a ship-fixed plane. The changing cross-sections of the ship from plane to plane add the extra half dimension to the solution. This extra half dimension shows up as a term that is proportional to the rate of change of added mass along the longitudinal axis of the ship. For each section, the sectional added mass can be calculated and then the longitudinal derivative determined. This longitudinal change in added mass is combined with the forward speed to produce a sectional vertical force. Each section is considered as an individual wedge impact problem, as illustrated in Figure 7.

The added mass of the wedge impact problem is given by the Wagner method [21] shown in Equation 2, with Pierson's hypothesis for the splash-up factor (Figure 8). In the LAMP formulation, the wetted beam with splash-up factor is not allowed to extend past the chines, as the flow will separate after that point.

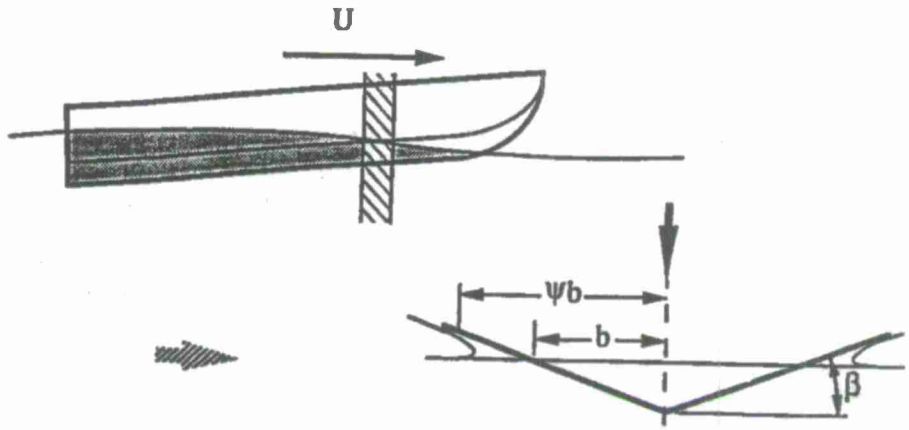

Figure 8: Dimensions of the Half-Wedge Impact Added Mass.

The 2.5-D method is also valid for calculating planing boat hydrodynamics in waves. The only difference is that the relative velocities between the sections and the water now contain terms from wave motion. By casting the impact problem for each section in ship-fixed coordinates and determining the wave motion also in ship-fixed coordinates, the sectional forces can easily be calculated just as they are for the calm-water case.

The restoring and incident wave forces are calculated by integrating the hydrostatic and Froude-Krylov pressure over the instantaneous wetted hull surface up to the incident wave waterline using the same body-nonlinear 3-D hull panel integration as for regular LAMP-2 and LAMP-4 calculations. Similarly, LAMP's plethora of external force and control system models for roll damping, appendages, propulsors, and the like can also be included in planing boat simulations. For planing boat simulations, these force models can also be used to account for hull lift not fully included in the 2.5-D model as well as active or passive trim tabs or other attitude control systems.

Highlight of Capabilities and Limitations

A major strength of the LAMP 2.5-D planing boat model is its computational speed – the hydrodynamic calculation is very fast and simulations can run much faster than real time unless a very large number of wave components are specified. The model is able to account for geometry variation in the longitudinal direction, and can treat stepped hulls approximately by sub-dividing the longitudinal cuts by step section. The theory also takes into account the splash-up of water on the hull in the wedge impact.

A weakness of the LAMP 2.5-D planing boat model is that the effects of transverse variations in the deadrise angle for a given section are not fully accounted for since they are represented as constant deadrise wedges. One aspect of planing boats where this effect is apparent is in spray rails and chine flats. Also, the LAMP planing boat model does not fully take into account 3-D effects such as the wake aft of the boat and the flow off the transom. It is a low-fidelity geometry model with the hull shape represented with a series of transverse equivalent wedges. Steps in the planing hull can be approximated so that longitudinal derivatives will not be taken across them (resulting in large spikes) but the air-water interaction effects will not be fully taken into account. Also, multiple chines, spray rails, and tunnels are not included in full detail.

Handling of Calm Water Sinkage and Trim

Due to the shallow angles between a planing hull and the water surface, small changes in heave and trim result in a large change in wetted surface area. Multiple seakeeping studies have shown that correcting the calm water heave and trim in the LAMP calculation to match that of the comparison craft will result in more accurate computations in waves. Noticeable variations in heave and trim result from small inaccuracies in the computed forces and moments. To correct the calm water heave and trim of planing boats in LAMP, additional forces and moments can be applied to the hull via numerical foils located below the center of gravity and the transom, in a manner similar to trim tabs. These foils account for the differences in the computed and actual forces and moments on the hull. The resulting corrected underwater volume and waterplane area lead to better prediction of the vessel's seakeeping performance. Since the foils move with the boat, the forces and moments will vary with the boat's orientation and with the incident wave. Results using these numerical tuning fins agree better with model test data than correction by a constant vertical force.

In a typical planing boat configuration, the numerical foils are sized to be similar in span as the beam of the boat. They are positioned horizontally near the keel, and the chord is such that the required angle of attack is about 10° or less, so that the foil's lift and drag are not based on a stalled foil. Figure 9 shows a setup of these numerical foils on the 20° deadrise prismatic hull.

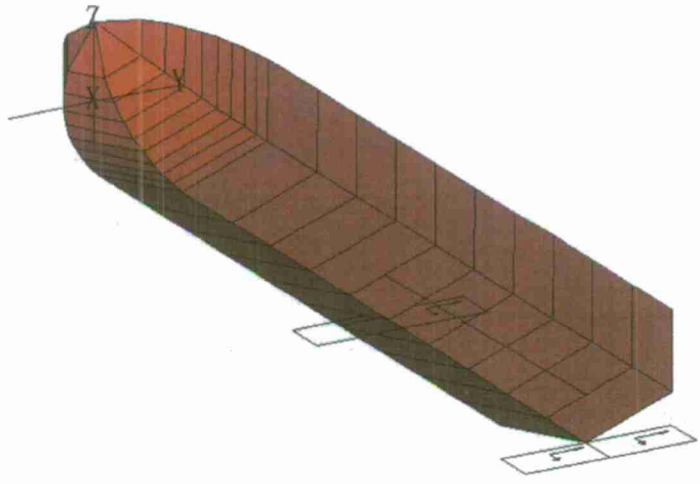

Figure 9: 20° Prismatic Model Showing the Numerical CG and Trim Tab Foils

VALIDATION PART 1: WEDGE DROP

The structural response of a planing boat during a slamming event is of interest to designers. In particular, the fatigue life of the structural members of existing planing boat designs are observed to be shorter than expected given current design tools. During a slamming event, the bottom of a planing hull experiences a severe pressure pulse as the spray root moves outboard from the keel. To quantify this high speed high pressure pulse, a wedge drop experiment was performed at the Naval Surface Warfare Center, Carderock Division (NSWCCD), the details of which can be found in Lesar et al [22] and Jiang et al [12]. The wedge was instrumented with an array of high frequency pressure gauges, which captured the pressure over time at various distances from the keel during impact. Both NFA and LAMP simulations were generated to replicate this experiment.

NFA Results

To assess NFA's ability to accurately predict these pressures, simulations of the experiments were performed. Care was taken to insure the initial conditions and boundary conditions were matched to the experimental setup. The wedge was dropped from rest at 6 in (15.24 cm) and 10 in (25.4 cm) above the undisturbed free surface. The model tank and the NFA domain were 15 ft (4.6 m) wide by 24 ft (7.3 m) long by 14.5 ft (4.4 m) deep. The wedge weighed 165.2 lbs (75 kg) and was 36 in (91.4 cm) by 23.75 in (0.60 cm) with a deadrise angle of 10.23 degrees. Figure 10 shows the bottom of the instrumented wedge alongside the NFA simulation's geometry and domain extents. Two symmetric pressure probes were located at 1.5 in (3.8 cm) from the keel. A four by four array of pressure probes had lines of 4 probes at 5.385, 6.795, 8.205, and 9.615 in (13.68, 17.26, 20.84, and 24.42 cm) from the keel. Each probe in the array was 1.41 in (3.58 cm) from its neighbor longitudinally and transversely. For both drop heights the NFA simulations used wall boundary conditions in each Cartesian direction. The number of grid points in the x, y and z directions was 1536, 1024, and 512, resulting in 805 million cells. Grid spacing near the wedge was 0.001L or 0.035 in (0.09 cm), where L is the wedge length. The non-dimensional time step taken was 0.00005, resulting in an output frequency of 37.8 KHz. The simulations were run on Jade, a Cray XT5, using 768 processors and took 12 hours for the 6 in (15.24 cm) drop height, running for 2000 time steps, and 32 hours for the 10 in (25.4 cm) case, running 6000 time steps.

The pressure probe measurements are plotted against the pressure predicted by NFA in Figure 11and in Figure 12, for the 6 in (15.24 cm) and 10 in (25.4 cm) drop heights respectively. The x-axis is time in seconds and the y-axis is gauge pressure in psi. Pressure-time histories from three completely separate drops are plotted together, with the peak from the first row of gauges aligned. The dashed black lines show 5 peaks in time, the first from the symmetric keel gauges and the remaining four from the four rows of pressure gauges in the array. Since the pressure pulse is quasi-2D, each row of pressure gauges in the keel-wise direction shows approximately the same time history. The time histories exhibit variability associated with minor experimental irregularities. The blue error bars represent the min and max of the experimental peaks for the 3 drops. The sampling frequency of the pressure probes was 19.2 KHz, while NFA pressures were extracted at a rate of 37.8 KHz. The peak from NFA's first row of gauges was aligned to the peak from the experiments and plotted in red. NFA shows excellent agreement for peak pressure magnitudes and pulse duration. The spray root takes approximately ten milliseconds to travel across the array of gauges and each peak pressure is maintained for less than 1ms. The propagation in time of the pressure pulse from the spray root is slowed by the deceleration of the wedge due to the impact with the free surface. The length of time between the final two peaks is therefore greater than that of the preceding peaks. NFA correctly predicts this momentum transfer

and thus the position in time of all four pressure peaks. NFA is within experimental variability for peak pressure and timing. It is notable that NFA also predicts the brief negative pressures seen in the experiments before the peak pressure due to the turbulent breakup of the expanding spray root.

Figure 13 and Figure 14 show image time sequences from the 6 in (15.24 cm) and 10 in (25.4 cm) drop height simulations, respectively. The camera is looking up at the wedge from underneath the water surface. The wedge is painted with contours representing the pressure that NFA has calculated. Blue represents zero pressure while red indicates 15 psi (103.4 kilopascals). The pressure pulse can be seen moving outboard from the keel over the pressure probes indicated by white dots on the bottom of the wedge on the right side. This pulse is concentrated at the spray root which can be seen as the translucent surface that begins to break up later in the simulation.

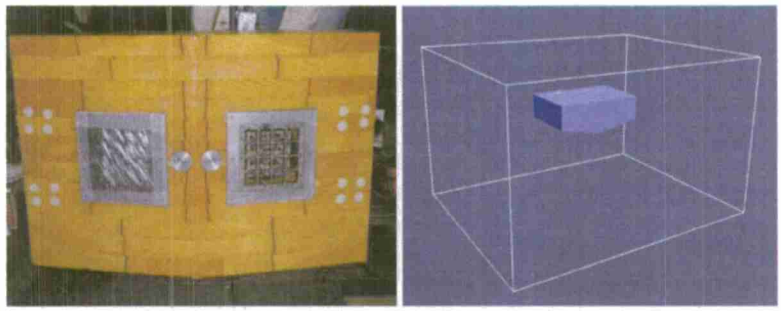

Figure 10. Photograph of instrumented wedge used in experiment on the left and NFA wedge geometry and domain size on the right.

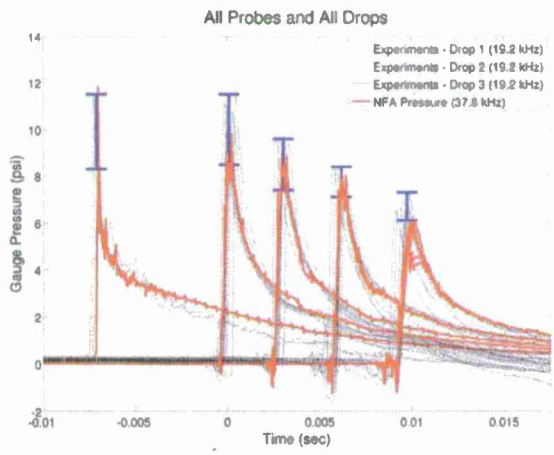

Figure 11. 6 in (15.24 cm) drop height case - NFA pressure predictions plotted on top of pressure gauge output from 3 separate drops.

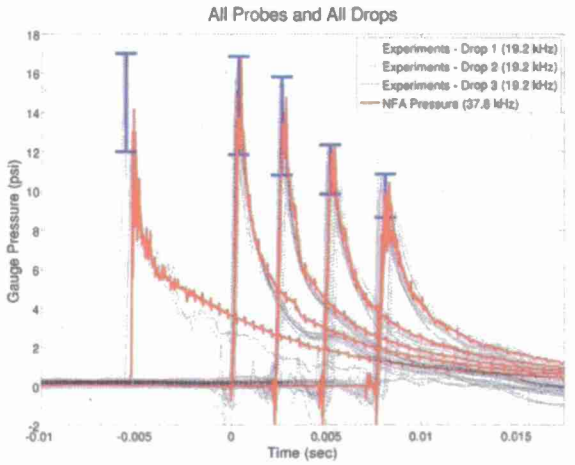

Figure 12. 10 in (25.4 cm) drop height case - NFA pressure predictions plotted on top of pressure gauge output from 3 separate drops.

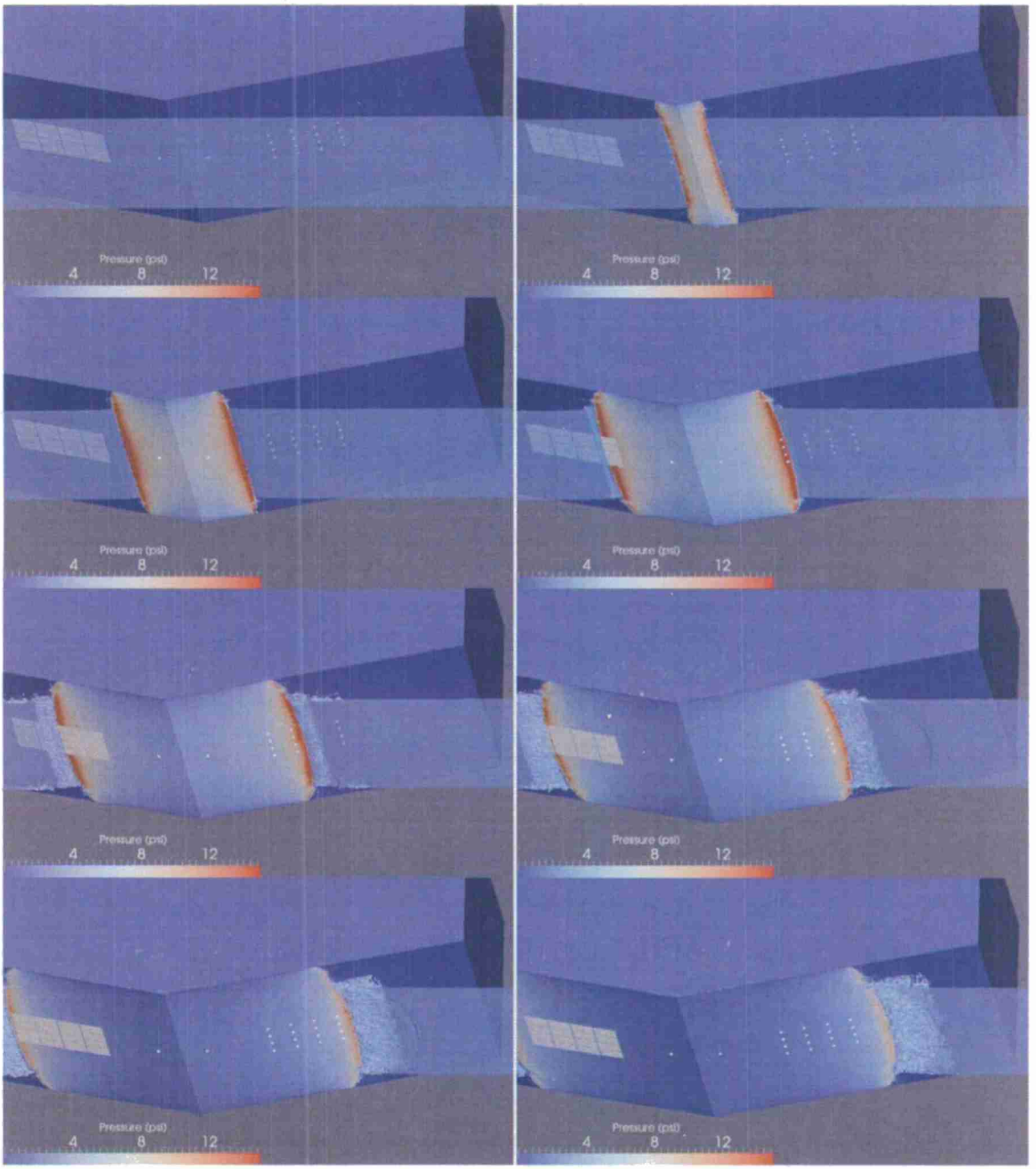

Figure 13. Time sequences of frames from an animation of the 6 in (15.24 cm) drop height wedge impacting the free surface. Pressure is interpolated onto the wedge and displayed, blue indicating 0 pressure, and red indicating 15 psi (103.4 kilopascals). Note the pressure wave from the spray root expanding transversely over the pressure gauges.

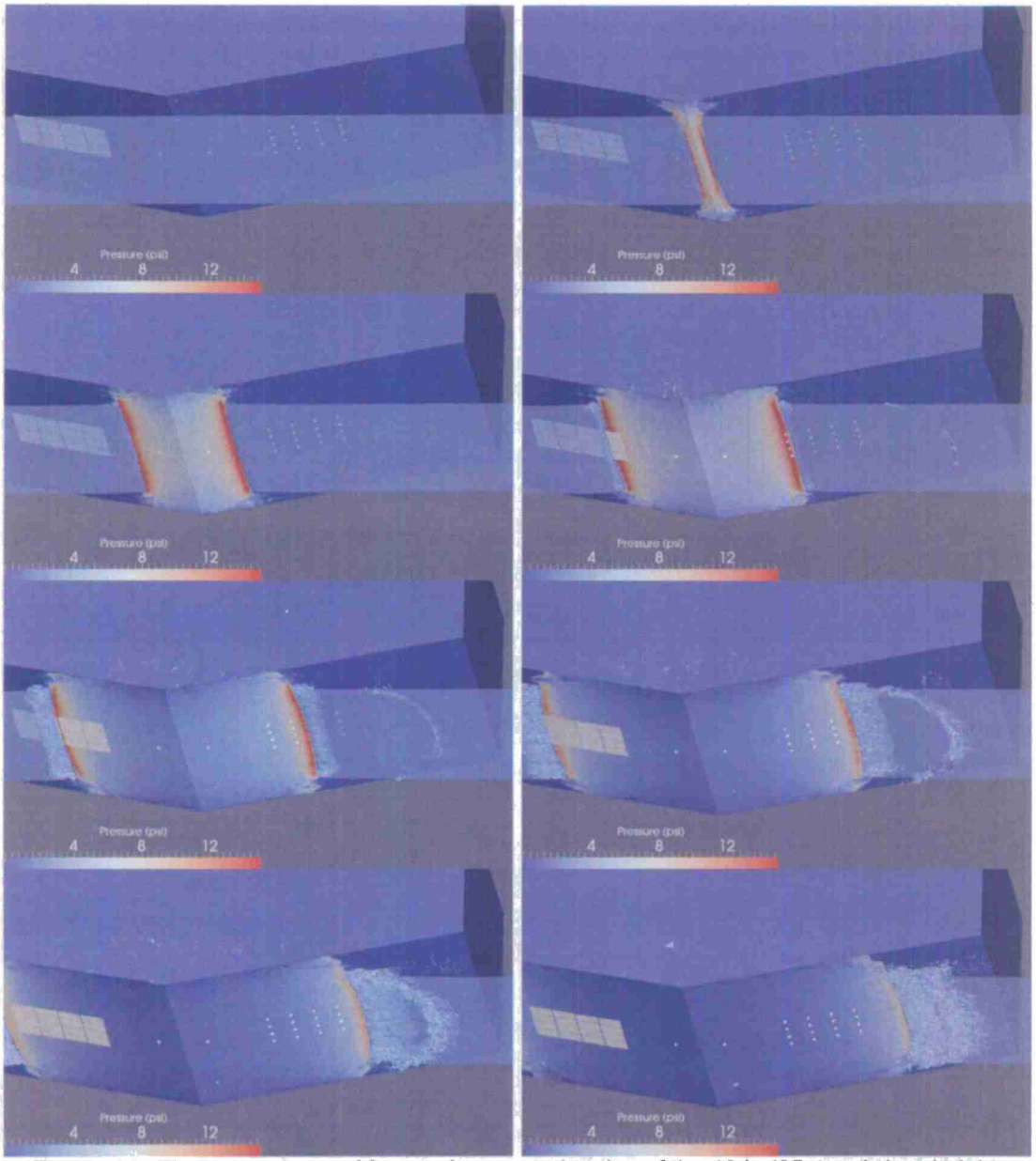

Figure 14. Time sequences of frames from an animation of the 10 in (25.4 cm) drop height wedge impacting the free surface. Pressure is interpolated onto the wedge and displayed, blue indicating 0 pressure, and red indicating 15 psi (103.4 kilopascals). Note the pressure wave from the spray root expanding transversely over the pressure gauges.

LAMP results

To evaluate the LAMP code with a setup similar to the same experiment, a set of forced-motion LAMP simulations were set up in which the 10° wedge starts just above the free surface and moves downward at a constant velocity. Figure 15 and Figure 16 show the body plan and perspective views, respectively, of the LAMP wedge model. LMPOUND impact calculations

were made with the wedge added mass finite-difference approach, the Richard Lewis effective pressure equation, Wagner's analytical expression for the pressure distribution for a 2D wedge, and SLAM2D, as described above.

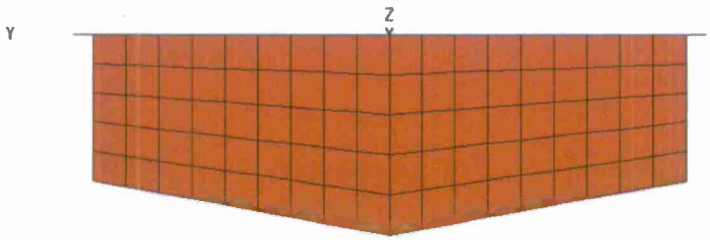

Figure 15. Body plan view of 10° wedge LAMP model.

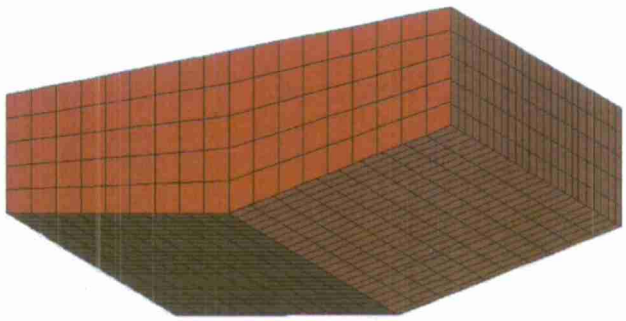

Figure 16. Perspective view of 10° wedge LAMP model.

The results for the implementation of the wedge added mass and Rich Lewis effective pressure are shown in Figure 17 as a function of impact velocity. Two of the curves are independently obtained using an Excel spreadsheet in order to double-check the LMPOUND results. The short red dash lines are pressure values obtained from experimentally measured structural responses. It can be seen clearly that the pressure obtained using the added mass method is higher than the pressure from the Richard Lewis approach.

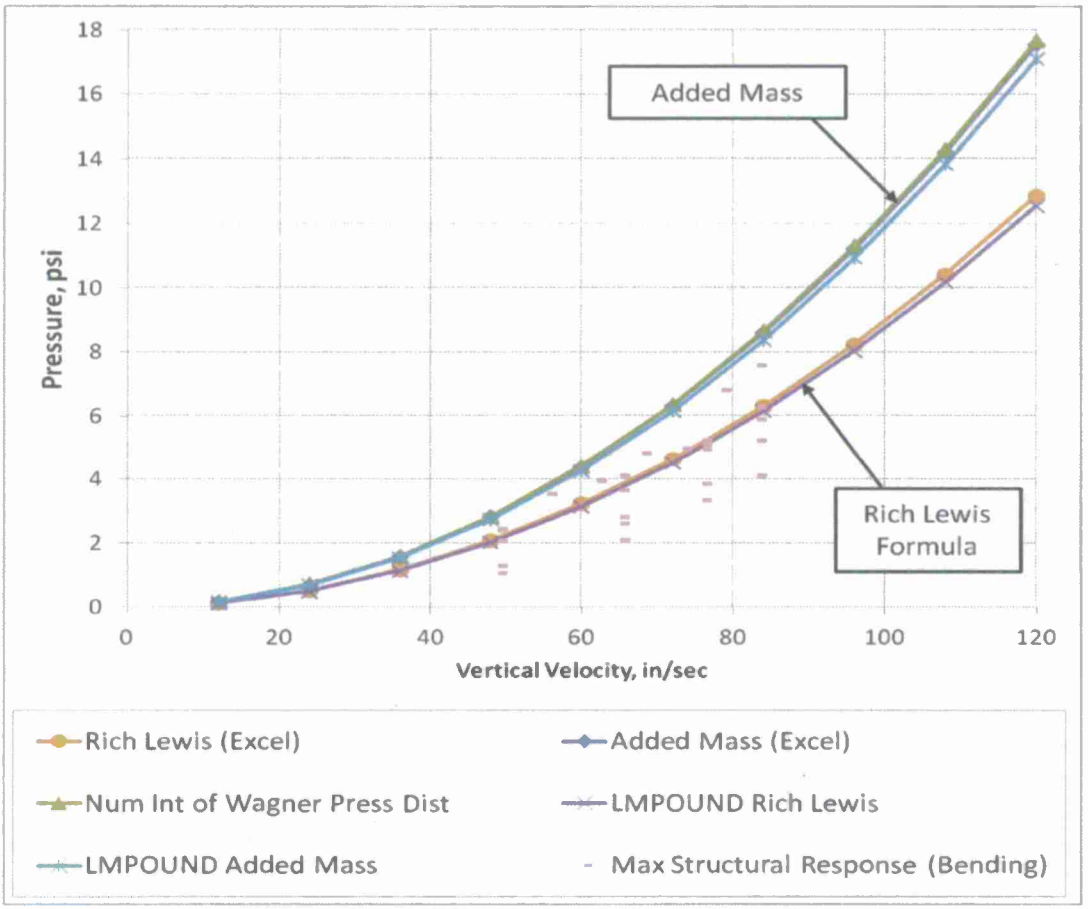

Figure 17. 10° Wedge impact LMPOUND results.

The normalized pressure distribution using Wagner's average pressure, Wagner's formula, and SLAMD2D are given in Figure 18. The plot shows that the SLAM2D method and the Wagner's formula predicted almost the same pressure distribution for this wedge case. While the wedge approximation method does not produce pressure directly, an average pressure derived from the impact forces is consistent with the average pressure computed using the Wagner formula and is a reasonable characterization of the pressure distribution of the wedge.

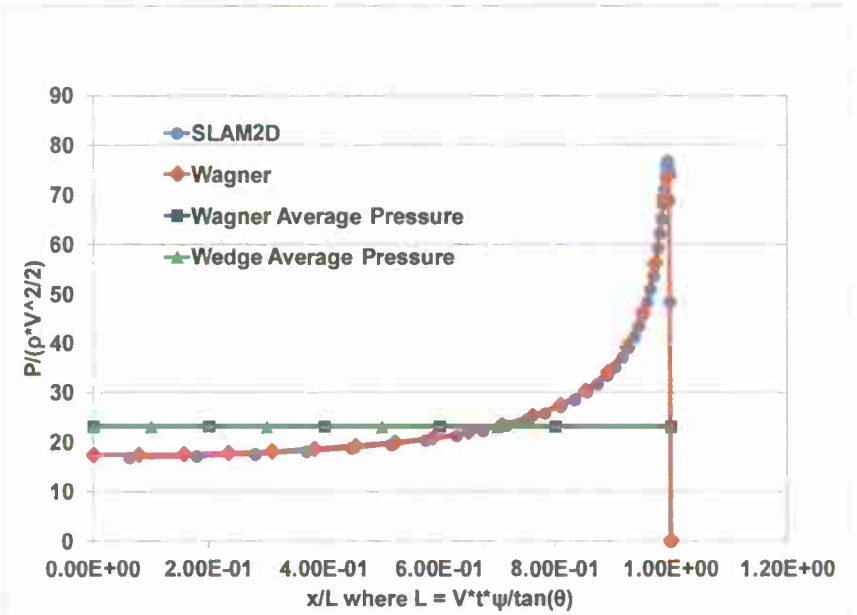

Figure 18. Normalized impact pressures of a 10° wedge using different methods: SLAM2D, Wagner, Averaged Wagner and Averaged Wedge.

A time history of the impact force calculated using the wedge formulation and the Wagner's formula are given in Figure 19. As can be seen, the wedge approximation has a spike in the force time history. This may be caused by time discretization and can potentially cause inaccuracy in motion response calculation.

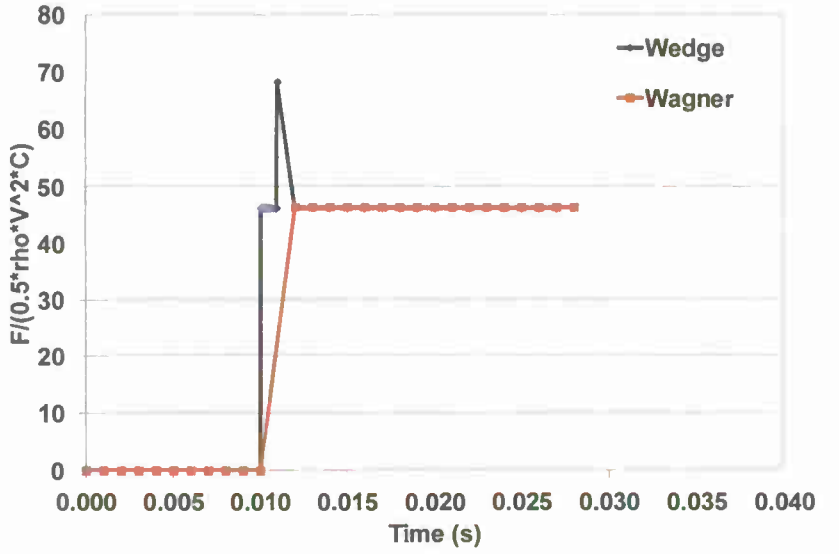

Figure 19. Normalized impact force of a 10° wedge.

VALIDATION PART 2: CONSTANT DEADRISE, STEADY FORWARD SPEED

In 1969, Fridsma [1] performed a tank test at the Stevens Institute of Technology using three models with constant deadrise of 10, 20, and 30 degrees, with length (L) to beam (b) ratios. NFA simulations were performed to replicate some of the runs from this experiment.

For NFA, three configurations with different length to beam ratios, L/b=4 and L/b=5 (shown in Figure 20 (left)), and light/heavy displacements are investigated. In all the simulations the model is of unit length with the bow of the model fixed at x=0, and the flow is from positive x. The model was free to sink and trim about the center of gravity (CG). The vertical center of gravity (VCG) was fixed at 0.294b above the keel, while the longitudinal center of gravity (LCG) was fixed at 0.6, 0.655, or 0.7 ship lengths from the bow. Inflow and outflow boundary conditions are used in the stream-wise (x) direction, and free-slip conditions are used in the span-wise (y) and cross-stream (z) directions. The inflow condition is a free-stream current, and the outflow condition is one-dimensional, non-reflective, Orlanski-type boundary condition. The Froude number is $Fr=U/\sqrt{(gL)}$, where U and L are respectively the speed and length of the planing hull model, and g is the acceleration of gravity, so Fr varies between 0.6 and 1.8 . The extents of the computational domain, shown in Figure 20 (right), in the stream-wise (x), span-wise (y), and cross-stream (z) directions are respectively [-3.0L, 1.0L], [-1.6L, 1.6L], and [-1.25L, 1.0L]. These dimensions were chosen to match the Davidson Laboratory's Tank 3 dimensions [23]. The number of grid points [nx, ny, nz] are [768, 512, 384]. The grid is stretched with nearly uniform spacing around the hull where the grid spacing is [0.00304L, 0.00306L, 0.00305L]. The maximum grid spacing far away from the ship along the Cartesian axes is [0.016L, 0.0204L, 0.0152L]. The grid points are distributed in 64x64x64 blocks over 576 cores, and the time step is $\Delta t=0.0005$. All simulations have been run on the Cray® (Cray Inc.) XE6, Raptor, platform located at the U.S. Army Engineering Research and Development Center (ERDC) and run by the Air Force Research Laboratory (AFRL).

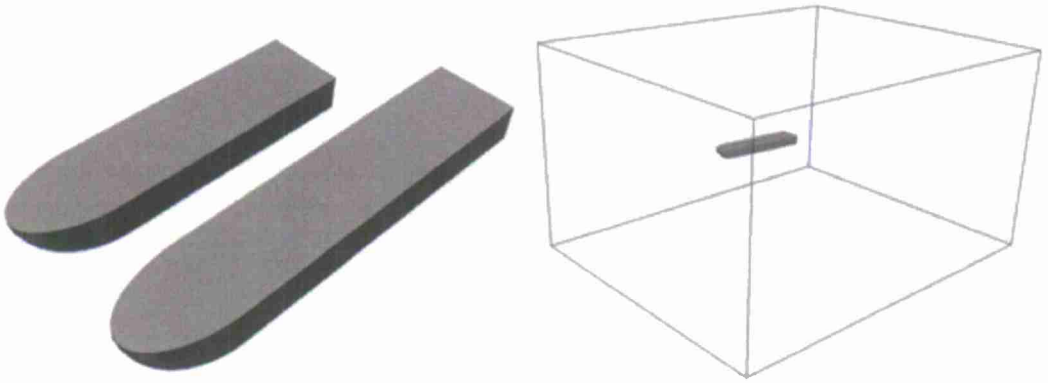

Figure 20. Setup L/b=4 and L/b=5 hull geometries (left) and L/b=5 model in computational domain (right).

Figure 21, Figure 22, and Figure 23 are comparisons of the sinkage or rise at the CG, on the left, the trim in the middle, and the ratio of the resistance to the displacement on the right. A ▲ denotes the experimental measurements made by Fridsma [1]; the ● denotes the predicted value according to Savitsky [2]; and the ■ denotes the value predicted by the NFA Simulations. The NFA simulations were averaged from T=4-8 for Figure 21 and Figure 22 and over the last

two boat lengths for Figure 23. The error bars show the minimum and maximum values over the averaging period for the rise at the CG and trim, and ± the r.m.s. for the resistance. The comparison of interest here is between the experiments and the NFA simulations, the Savitsky predictions are simply provided for completeness.

Figure 21 shows the results of the comparison for C_Δ=0.608, L/b=4 and β=20°, with the LCG at 0.6L from the bow. Where C_Δ is the load coefficient defined as $C_\Delta = \Delta/(wb^3)$, where Δ is the hull displacement, w the specific weight of water, b is the beam of the hull, L is the length of the hull, and β is the deadrise angle. The rise at the CG, shown in hull lengths, is shown (left) at the slower speed ratios, $VL^{-1/2}$ [knots-ft$^{-1/2}$], namely two and three, the results of the simulations are identical to those recorded during the experiments. At higher speed ratios, namely four, five and six, the rise at the CG is under predicted by the simulations. The trim, shown in the middle frame, shows good agreement with the experiments, although again at the higher speeds, the simulations under predict the final trim angle by around ten percent. It is noted that the general shape of the curve matches the shape of the curve recorded in the experiments and also the predictions from Savitsky. The resistance (right) is under predicted for all but the highest speed case, where it is over predicted. In all three frames of Figure 21, the error bars are small, meaning that the simulations predicted a nearly constant value for the quantities of interest. No porpoising was observed.

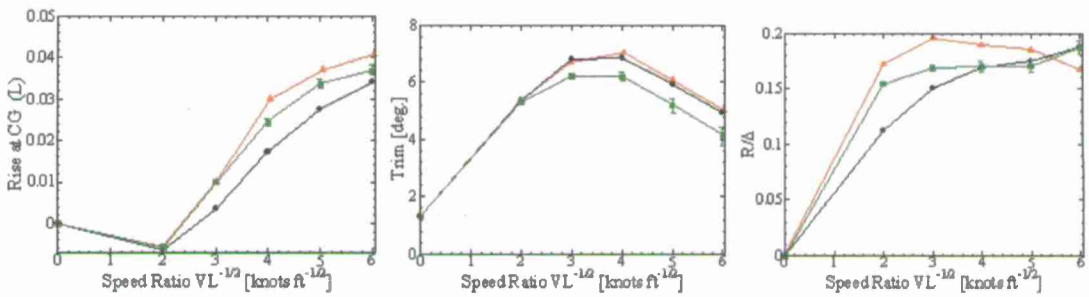

Figure 21. Fridsma comparison for C_Δ=0.608, L/b=4 and β=20°. ▲, Fridsma Experiments[1]; ●, Savitsky Predictions [2]; ■, NFA Simulations. Rise at the CG (left), trim (middle), and resistance (right).

Figure 22 shows the results of the comparison for C_Δ=0.608, L/b=5 and β=20°, with the LCG at 0.655L from the bow. The rise at the CG, shown on the left, is well predicted by the numerical simulations at the lower speed ratios. There is good qualitative agreement at the higher speeds, but again the numerical simulations under predict the rise at the CG at the higher speeds. The trim, shown in the middle, is well predicted by the numerical simulations, being nearly identical to the experiments for speed ratios of two and three. For the higher speed ratios, those above three, the trim is under predicted but the shape of the curve is similar to the one recorded in the experiments and the one predicted by Savitsky. The resistance, shown on the right, displays the opposite trend to the L/b=4 case. That is, it is over predicted by the numerical simulations for speed ratios between two and five, and then under predicted for a speed ratio of six. No porpoising was observed.

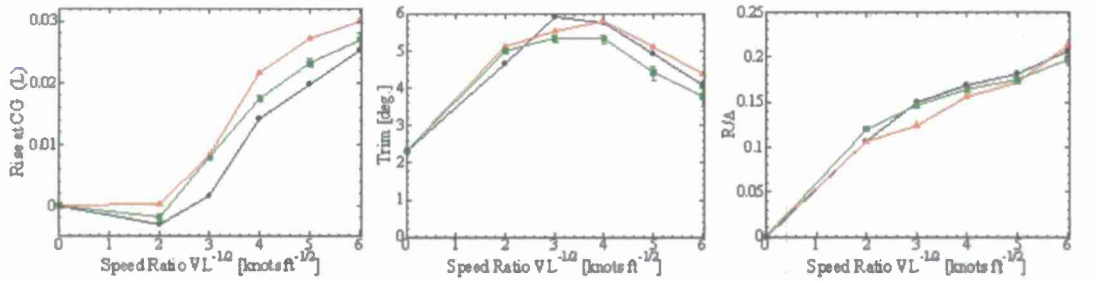

Figure 22. Fridsma comparison for C_Δ=0.608, L/b=5 and β=20°. ▲, Fridsma Experiments [1]; •, Savitsky Predictions [2]; ■, NFA Simulations. Rise at the CG (left), trim (middle), and resistance (right).

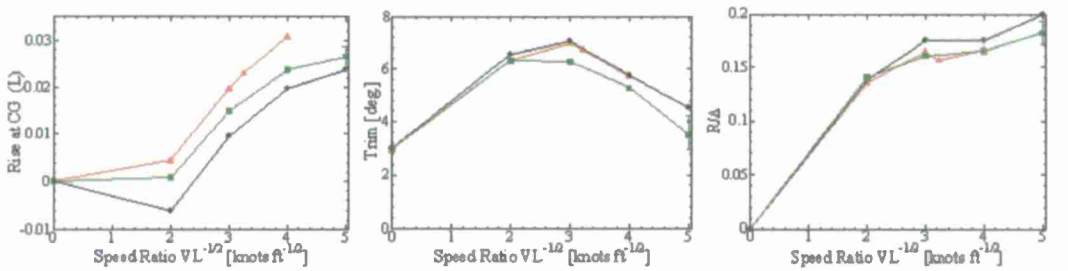

Figure 23. Fridsma comparison for C_Δ=0.304, L/b=4 and β=20°. ▲, Fridsma Experiments [1]; •, Savitsky Predictions [2]; ■, NFA Simulations. Rise at the CG (left), trim (middle), resistance (right).

Figure 23 shows the lighter displacement case for C_Δ=0.304, L/b=4 and β=20°, with the LCG at 0.7L from the bow. The rise at the CG, on the left, is under predicted over the entire speed range. Note the large error bars at the speed ratio of five. This case is the speed at which the model displayed evidence of porpoising in the experiments, and no data was recorded. The trim, shown in the middle, again shows excellent agreement with the value recorded in the experiments for the lowest speed ratio, two, but is under predicted for speed ratios of three and four. The resistance, shown on the right, is nearly identical to the values recorded in the experiments. Porpoising was observed at a speed ratio of five, which was consistent with the experiments.

Figure 24 shows the trim as a function of time as predicted by NFA. For speed ratios of two and three a steady trim is achieved after only two boat lengths. The speed ratio of four achieves a quasi-steady trim after about five boat lengths. However, the speed ratio of five does not achieve a steady trim and furthermore the amplitude of the oscillations does not decay with time.

Figure 25 shows NFA-predicted instantaneous pressures on the bottom of the hull for the C_Δ=0.608, L/b=4 and β=20°, with the LCG at 0.6L from the bow for speed ratios of two through six moving from left to right. The transition from displacement to planing is evidenced by the sharpening of the spray root and lack of hydrostatic pressure aft of the spray root, which can be observed by comparing the leftmost and rightmost frames. The hot spots are transitory in nature and would not be observed if a time averaged pressures were shown. Given their transitory nature, they do not significantly contribute to the force balance which determines the position of the hull.

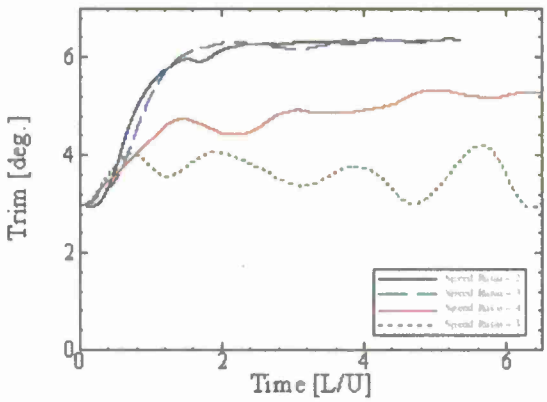

Figure 24. Trim versus time for C_Δ=0.304, L/b=4 and β=20°. Note the oscillatory behavior at a Speed Ratio of 5 (green line), indicative of porpoising. [Speed Ratio is in knots-ft-1/2].

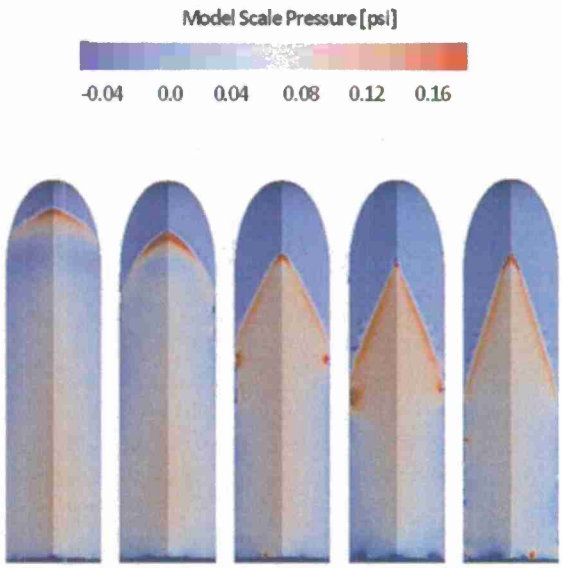

Figure 25. Pressures on hull for C_Δ=0.608, L/b=4 and β=20° Speed Ratio = 2, 3, 4, 5, 6 (from left to right).

LAMP

To replicate the experiments of Fridsma [1], three prismatic hull forms, with 10°, 20°, and 30° deadrise as shown in Figure 26, were simulated by LAMP at various conditions. The models have an overall length of 45 inches (1.14 m) and an overall beam of 9 inches (22.9 cm). As shown in Table 1, the longitudinal centers of gravity (LCGs) in the tested conditions are set so that the running trim in calm water is 4°, 5°, or 6°. Speed-length ratios of 2, 4, and 6 knots/ft$^{1/2}$ were covered, which correspond to model speeds from 3.87 to 11.62 ft/s (1.18 to 3.54 m/s). Two load coefficients (displacement divided by density, gravity, and beam cubed $[\frac{\Delta}{\rho g b^3}]$) were tested: load coefficients of 0.608 and 0.912 correspond to displacements of 16 and 24 lbf (7.3 and 10.9 kg), respectively. The height of the center of gravity is 2.646 inches (6.7 cm) above the keel.

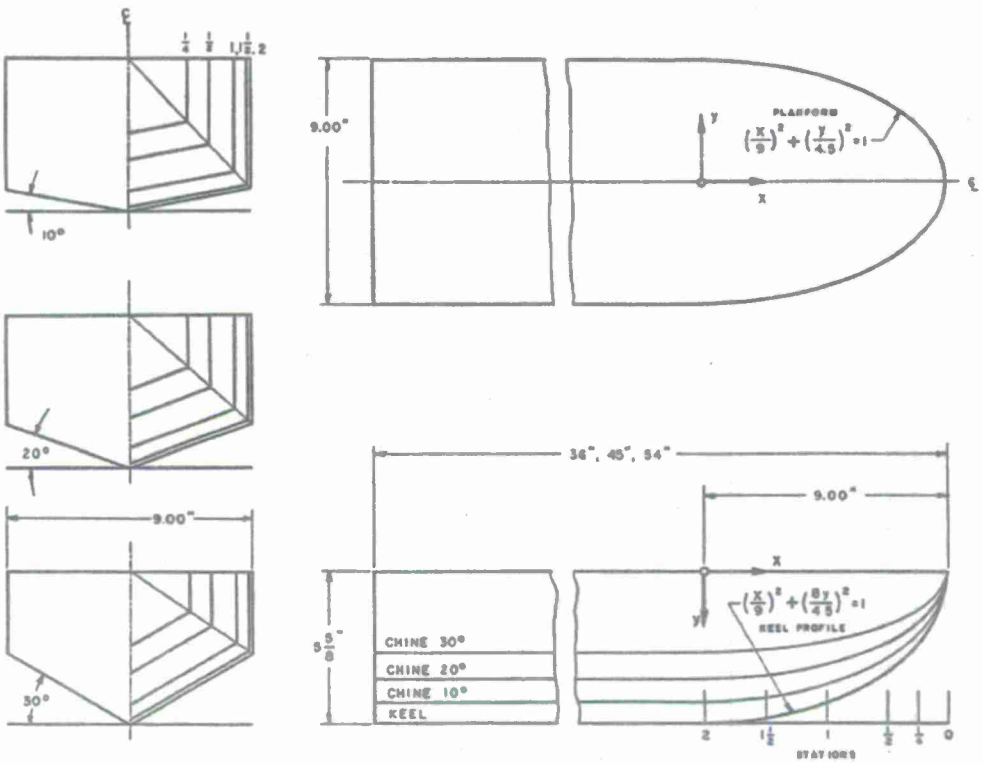

Figure 26: Lines Plan of the Three Fridsma Prismatic Planing Boats.

Table 1: Characteristics of the Prismatic Hull Forms.

Configuration	L/b	β (deg)	C_Δ $\left(\frac{\Delta}{\rho b^3}\right)$	LCG (%L)	Trim (deg)	Pitch Gyradius, k (%L)	$V/L^{1/2}$ (knots/ft$^{1/2}$)
A	5	20	0.608	59.0	4	25.1	4
B	5	20	0.608	62.0	4	25.5	6
C	5	20	0.608	61.5	4	25.3	2
D	5	20	0.608	67.5	6	26.5	2
E	5	20	0.608	65.5	6	26.2	4
F	5	20	0.912	58.0	6	20.4	4
G	5	20	0.912	58.0	5	20.4	6
H	5	10	0.608	62.0	4	25.6	2
I	5	10	0.608	59.5	4	25.0	4
J	5	10	0.608	68.0	4	26.2	6
K	5	30	0.608	61.0	4	24.7	4
L	5	30	0.608	62.5	4	24.9	2
M	5	30	0.608	60.5	4	24.8	6

Calm Water Results

Figure 27 and Figure 28 show the calm water results for the 13 tested configurations as compared to the model test results and Savitsky's method prediction [2]. The LAMP results with no tuning fins show that the model's heave is generally overpredicted as compared to the model test. This is especially true for low-speed cases, which is expected since the model is not fully planing in this regime. The calm water trims match up well and are generally within a degree of the model test result. Savitsky's method predictions are close to the model test and LAMP results. Savitsky's method tends to predict the slower speed heave more accurately than LAMP.

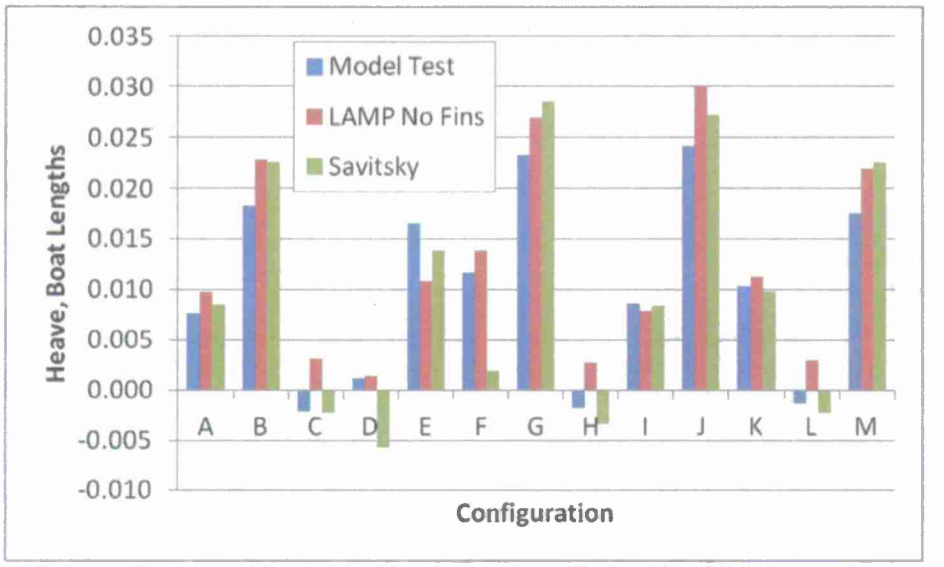

Figure 27: Heave Comparison for the Fridsma Planing Boat Configurations.

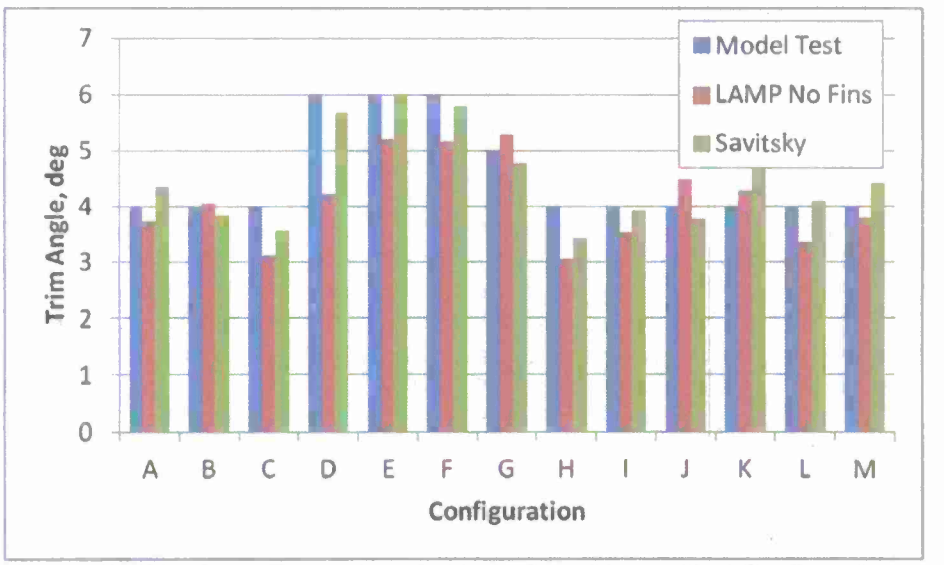

Figure 28: Trim Angle Comparison for the Fridsma Planing Boat Configurations.

Creste Wave Results

Heave and pitch response amplitude operators (RAOs) for the 13 cases are presented in Appendix A. The blue lines represent the model test data, the green lines are the LAMP results with no tuning fins, and the red lines are the LAMP results with tuning fins. Note that the LAMP results with tuning fins correlate better with the model test results for most of the configurations.

VALIDATION PART 3: FIXED ROLL COMPARISONS

Experimental Description

In order to investigate the transverse stability and to support the development of CFD codes for high speed, small-craft applications, the United States Naval Academy (USNA) performed a series of forced roll experiments on a prismatic planing hull [24]. An experimental mechanism to force a planing hull model in roll motion was designed and built. The Forced Roll Mechanism was intended to act as a dynamometer that forces a planing hull in roll and measures the resulting roll moment, as well as the heave and sway forces. The trim and rise of the model can be adjusted between test runs. The dynamometer can be configured to either oscillate the model or hold the model at a fixed roll angle, and measure the forces whether dynamic or static in nature, while allowing different testing conditions in terms of speed, rise and trim. A photograph of the system attached to a wooden 20 degree deadrise model, as well as an expanded detail of the forced roll mechanism is shown in Figure 29. The characteristics of the planing hull model are given in Table 2.

With the present motors and instrumentation, the Forced Roll Mechanism (FRM) system is capable of a maximum RPM of 150 (2.5 Hz) and a maximum roll amplitude of 30 degrees for the 20° deadrise wooden planing hull model. The roll angle amplitude is limited by the model clearance with the FRM support structure. Judge [24] showed that the roll added inertia calculation is highly sensitive to the error in the measured forcing moment amplitude at low frequency. Therefore, to accurately determine the coefficients in roll when oscillating at low frequencies, there must be tighter error control of the forcing moment measurements or an increased number of test runs.

By combining information from the various load cells in the FRM, the total heave and lift forces and roll moment can be determined The block force gauges attached to the supporting heave post assembly measure purely vertical and horizontal (sway) forces in the tow tank reference frame. However, the bi-axial load cell is attached to the model and, therefore, reads vertical and horizontal (side) forces relative to the model. Since the model is trimmed and rotating in roll, these measured forces need to be resolved to find the vertical and horizontal forces relative to the heave post assembly.

Testing was performed in the United States Naval Academy Hydromechanics Laboratory's 380 foot tow tank. The USNA tow tank is 380 ft (116 m) long with a width of 26 ft (7.9 m) and a depth of 16 ft (4.9 m). The model was tested at two displacements : 30.75 and 55 lbs (14 and 25 kg), three velocities: 20, 25 and 30 ft/s (6.1, 7.6, and 9.1 m/s), five fixed roll angles: 0, 5, 10, 15, and 20 degrees, three forced roll oscillation amplitudes: 10, 15 and 20 degrees, and three forced roll oscillation frequencies, up to 3 Hz. In addition to the roll position of the model, the heave and sway forces and the roll, yaw, and pitch moments during each test were measured [24]. The NFA validation effort focused on the first portion of this test; that is, the results for steady forward speed, at fixed sinkage and trim, at a series of different roll angles.

Figure 29. Images showing an overview of Forced Roll Mechanism and detail of the roll forcing design.

Table 2. Characteristics of USNA Planing Hull Model.

Length on the waterline	5 ft (1.524 m)	
Chine beam	1.48 ft (0.451 m)	
Deadrise	20 degrees	
Displacement	29.8 lb (13.5 kg)	58.4 lb (26.5 kg)
KG	5.29 in (13.44 cm)	
LCG (fwd transom)	12.0 in (30.5 cm)	23.4 in (59.4 cm)

The lift force, sway force, and roll moment were determined as a function of time for all the steady and dynamic roll tests. The nominal weight of the planing hull was taken to be the lift force from the steady zero-roll test. The fixed trim and heave for the model were determined from the zero-roll equilibrium trim and heave measured during a free to trim and heave run. This weight was used to non-dimensionalize the forces measured. The roll moment was non-dimensionalized by this weight times the beam of the model. The model velocity was non-dimensionalized by the beam Froude number, given by Equation (10):

$$Fr_B = \frac{V}{\sqrt{gb}} \tag{10}$$

where V= model velocity, g=gravitational acceleration, and b=beam width

Lift Force

The lift force was calculated from the total forces measured on the model in the direction perpendicular to the water surface. This direction was defined as 'vertical', meaning the lift was measured in a reference frame oriented with the water surface. The lift was measured while the model was towed at constant heel angles and during the dynamic roll tests. Figure 30 shows the lift force as a function of heel angle at three model speeds during the steady heel tests for two displacements. The lift force for the heavier displacement shows no speed dependence (right),

although the lift force increases with speed for the lighter displacement (left). The heavier displacement steady lift force shows little dependence on heel angle until heeling beyond the deadrise angle of the hull. However, the steady lift force does depend on heel angle for the lighter displacement, especially at the faster model speeds. Therefore, there can be a coupling between heave and heel, at least when the vessel is running lightly loaded.

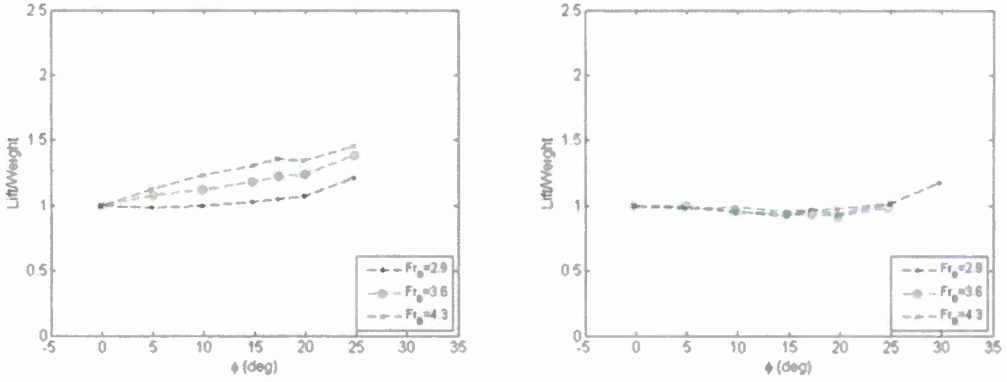

Figure 30. Lift force for steady roll angle model tests; lighter displacement (left) and heavier displacement (right).

□*ette*□*Le*□□*t*□□

The keel wetted length is defined as the distance from the transom along the keel to where the keel is first wetted. The chine wetted lengths are defined as the distance from the transom along the chine to where the chine is first wetted. Figure 31 shows an underwater photograph of the model with the wetted lengths labeled.

Figure 31. Underwater photograph of the model showing the different wetted lengths (Fr_B = 4.3, roll angle = 10°).

Savitsky [2] provides wetted length predictions for steady planing hulls with no roll angle. However, there is no currently available method for predicting wetted lengths for hulls experiencing roll, even for steady planing. Wetted length is important for determining the hydrodynamic forces on a planing hull. Therefore, it is critical to understand the difference in wetted length due to roll angle or dynamic motion. Figure 32, Figure 33, and Figure 34 show the keel, starboard chine, and port chine wetted lengths for three different model speeds as a function of roll angle for the steady heel tests. The keel wetted length does not vary significantly with heel angle, while the port and starboard chine wetted lengths show opposite trends. As would be expected, the starboard and port chine wetted lengths are close to equal at zero heel. As the model heels to starboard, the starboard chine wetted length increases and the port chine wetted length

decreases. Eventually the starboard chine wetted length equals the keel wetted length and the port wetted length becomes zero. When the model is heeled to 20 degrees, the bottom of the model is flat from the keel to the chine since the deadrise is 20 degrees. For this condition, it is to be expected that the starboard and keel wetted lengths are equal. This is the case for the lighter displacement, but for the heavier displacement scenario shows the keel wetted length still greater than the chine wetted.

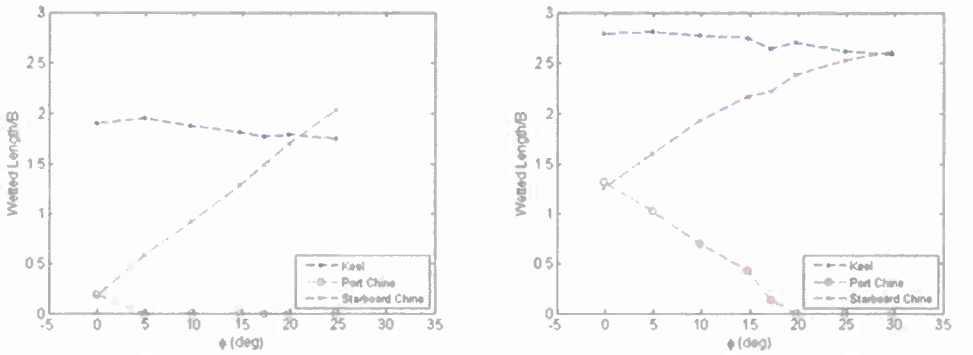

Figure 32. Steady Heel – Keel, starboard and port chine wetted lengths for model speed Fr_B = 2.9; lighter displacement (left) and heavier displacement (right).

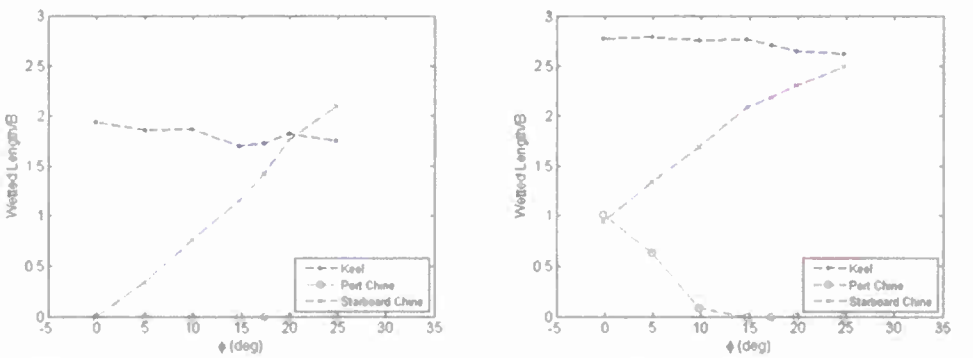

Figure 33. Steady Heel – Keel, starboard and port chine wetted lengths for model speed Fr_B = 3.6; lighter displacement (left) and heavier displacement (right).

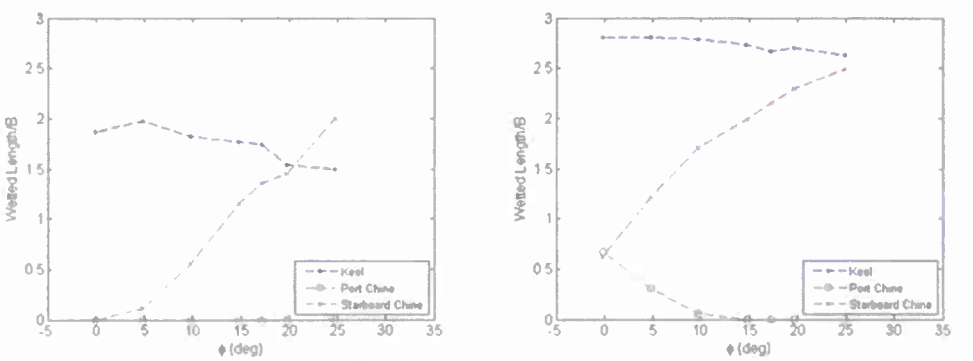

Figure 34. Steady Heel – Keel, starboard and port chine wetted lengths for model speed Fr_B = 4.3; lighter displacement (left) and heavier displacement (right).

The keel wetted length shows a slight decrease as steady roll angle increases. This is likely because the model was fixed in heave and rotated about an axis through the model's center

of gravity. As the roll angle becomes large, the keel moves up slightly resulting in a decrease in keel wetted length. The port wetted length is zero if the spray reaches the transom before reaching the chine. Figure 35 shows a photograph demonstrating zero chine wetted lengths.

Figure 35. Underwater photograph of the model showing zero chine wetted lengths (Fr_B=4.3, zero roll angle).

The wetted lengths can be different for the same roll angle when the model is experiencing dynamic roll. As the model rolls to starboard, it would be expected that the starboard chine wetted length would increase compared to the same angle at zero roll angle and the port chine wetted length would decrease comparatively. The keel wetted length should not be significantly affected by the roll motion. Figure 36 and Figure 37 show the keel and starboard chine wetted lengths as a function of roll angle for the steady and dynamic roll angles for a single model speed. The dynamic wetted lengths include measurements from all roll amplitude and roll oscillation frequencies tested. As expected, the keel wetted length is relatively constant for both the steady and dynamic tests. The dynamic motion of the model does not significantly affect the wetted portion of the keel. The chine wetted lengths also show little variation due to dynamic roll motion.

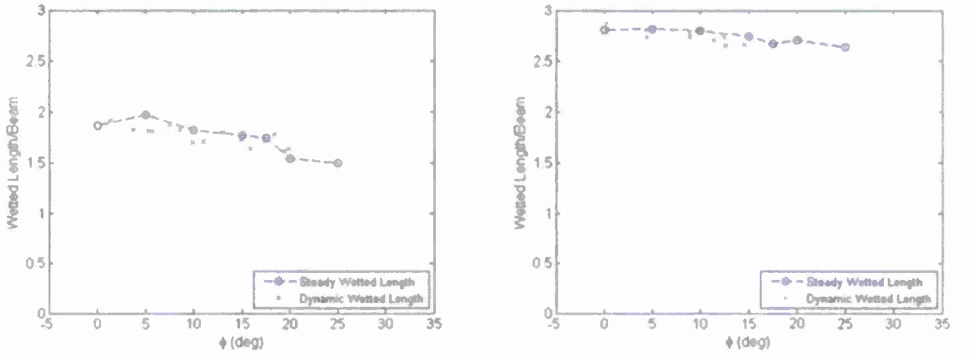

Figure 36. Steady and dynamic roll keel wetted Lengths for model speed Fr_B = 4.3; lighter displacement (left) and heavier displacement (right).

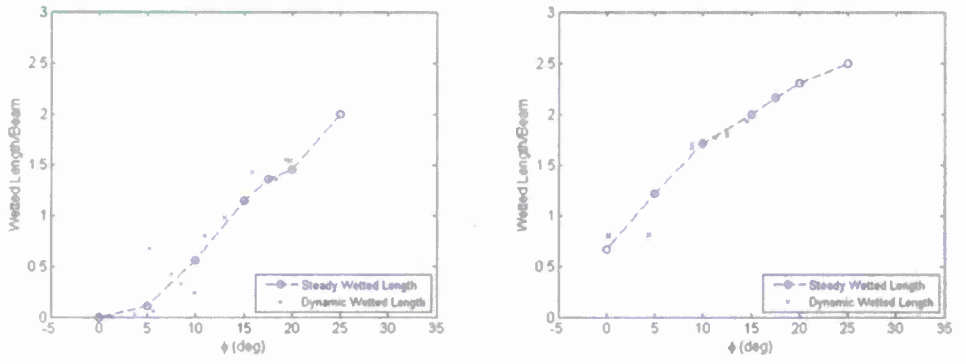

Figure 37. Steady and dynamic roll starboard wetted lengths for model speed Fr_B = 4.3; lighter displacement (left) and heavier displacement (right).

NFA Comparison

The NFA validation effort focused on the steady roll portion of the test, that is, the NFA simulations were performed only for the steady roll cases. The USNA geometry and NFA's domain can be seen in Figure 38. Four cases of varying roll angles (0, 10, 20, and 30 degrees) at 20 ft/s (6.1 m/s) were investigated. The geometry was positioned at a trim of 4 degrees and a draft at the transom of 3.574 in (9.08 cm), and then rolled around an axis parallel to the keel at the VCG of 5.29 in (13.44 cm). The simulation was run with a width of 2 boat lengths, or 10 ft (3.05 m) and a depth of 1 boat length, or 5 ft (1.52 m). NFA's domain had to be smaller than the towing tank to cluster cells near the body without stretching the grid too heavily. This smaller domain may have resulted in some blockage and further simulations need to be performed to investigate the effect of domain size. The number of cells in x, y, and z was 1280, 896, and 448, resulting in 514 million cells in the total simulation. Spacing near the body was 0.0009L or 0.054 in (0.137 cm), necessitating a non-dimensional time step of 0.00023. Simulations were run for 13,000 time steps, or 3 body lengths, which was sufficient to reach steady state, on Garnet, a Cray XT6 at ERDC and took approximately 24 hours to complete using 576 processors.

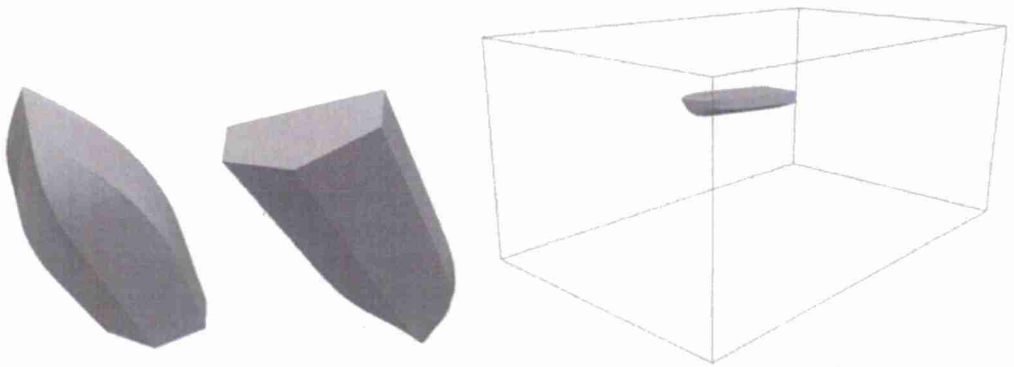

Figure 38. USNA Constant deadrise hullform (left) and NFA setup with geometry and domain extents (right).

Figure 39, Figure 40, Figure 41, and Figure 42 show the underwater photographs taken during the experiments compared to a similar view of the NFA simulations for each roll angle at 20 ft/s. The spray root line, and thus wetted surface area appear to agree with the experiments qualitatively at the lower speeds, with lower agreement at higher speeds. The spray sheet appears to extend further than the NFA prediction, particularly for the higher speeds. NFA

models the instabilities in the spray sheet breakup reasonably well. As the model rolls over the flow over the chine initially separates cleanly, but at 20 degrees and higher the flow wraps around the chine and wets the side of the model. The NFA simulations exhibit this behavior as well.

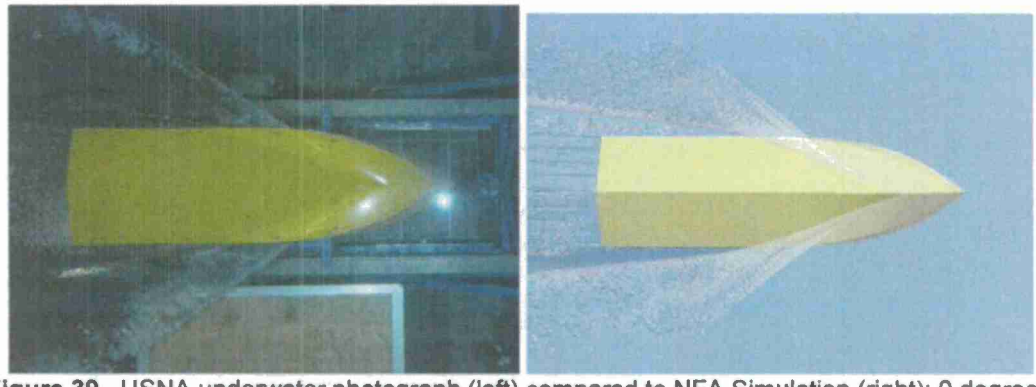

Figure 39. USNA underwater photograph (left) compared to NFA Simulation (right); 0 degrees roll, U=20 ft/sec.

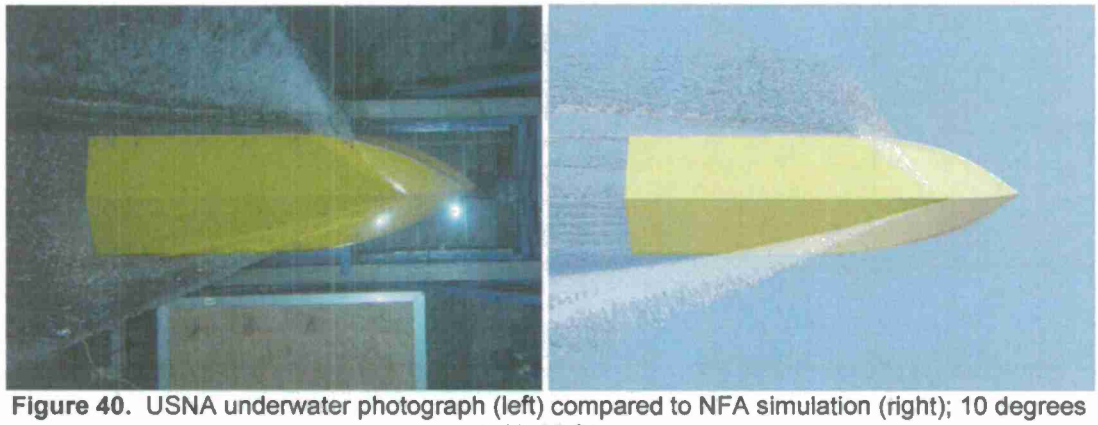

Figure 40. USNA underwater photograph (left) compared to NFA simulation (right); 10 degrees roll, U=20 ft/sec.

Figure 41. USNA underwater photograph (left) compared to NFA simulation (right); 20 degrees roll, U=20 ft/sec.

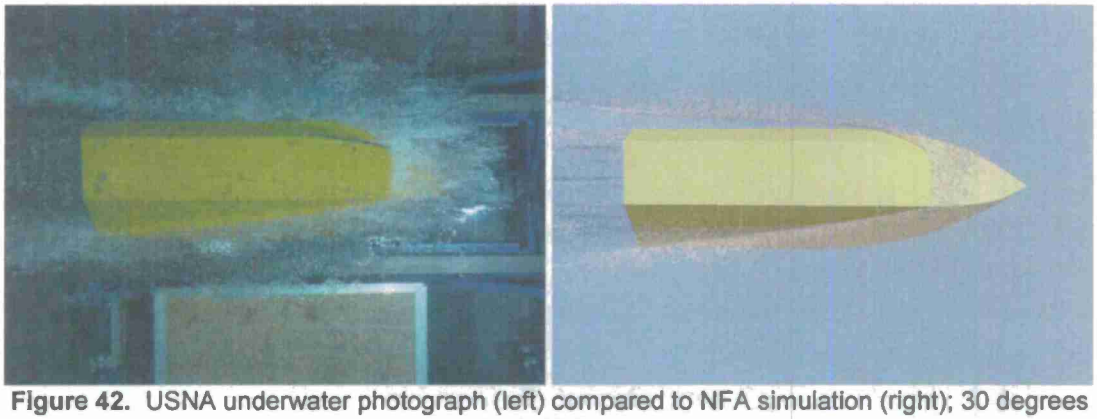

Figure 42. USNA underwater photograph (left) compared to NFA simulation (right); 30 degrees roll, U=20 ft/sec.

The bottom of the model was painted with a ruler and the lengths along the keel and chines were estimated from the underwater pictures. The same values were extracted from the NFA results and the comparison is plotted in Figure 43. The agreement is excellent throughout the range of roll angles. It follows that wetted surface area is being accurately predicted as well.

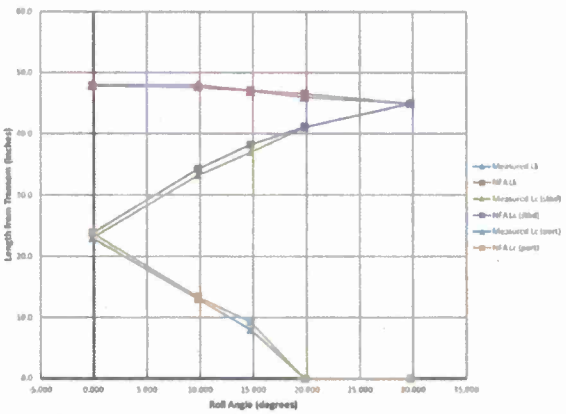

Figure 43. Comparison of NFA results to experiments for length along the keel, length along the starboard chine and length along the port chine for each roll angle simulated. Lengths are measured in inches from the transom.

LAMP Comparison

The USNA planing boat model tested was also modeled in LAMP and compared to experimental data at two displacements. Figure 44 shows two perspective views of the LAMP input geometry for USNA planing boat.

Figure 44. Perspective Views of the USNA Planing Boat LAMP Model.

Calm Water Results

Figure 45 and Figure 46 show the calm water heave and trim for the experiment, Savitsky's method prediction, and the LAMP model. Note that with the given geometry and center of gravity location, the zero-speed trim for the 30.75 lb displacement model was calculated to be 5.55°. This is 0.6° greater than the 4.95° trim reported. This discrepancy does not seem to have much effect on the at-speed results. Generally, the LAMP results compare well with the model test and Savitsky method results for calm water heave and trim. For the heavy displacement model, trim of the LAMP model is about a degree less than the model test and Savitsky method results, but the heave corresponds well at that displacement.

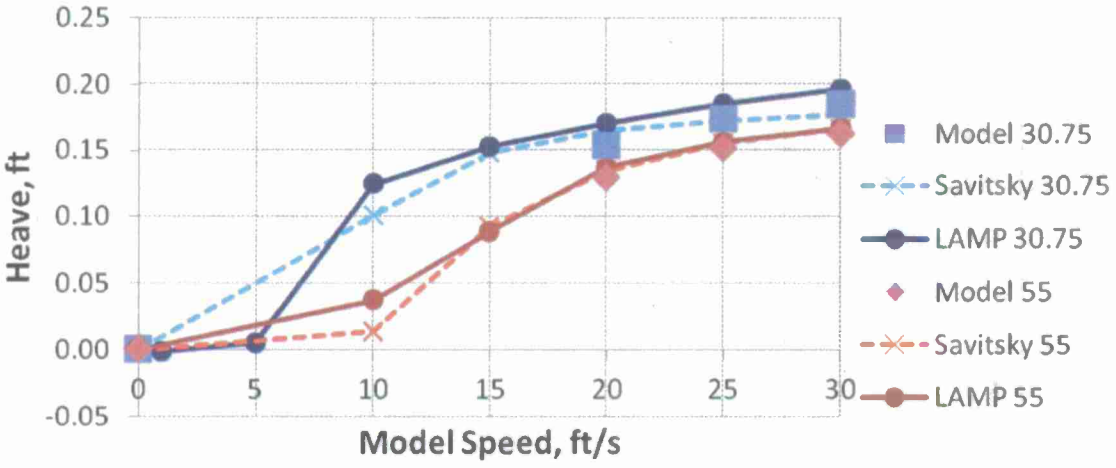

Figure 45. USNA Model Heave versus Speed for Two Displacements.

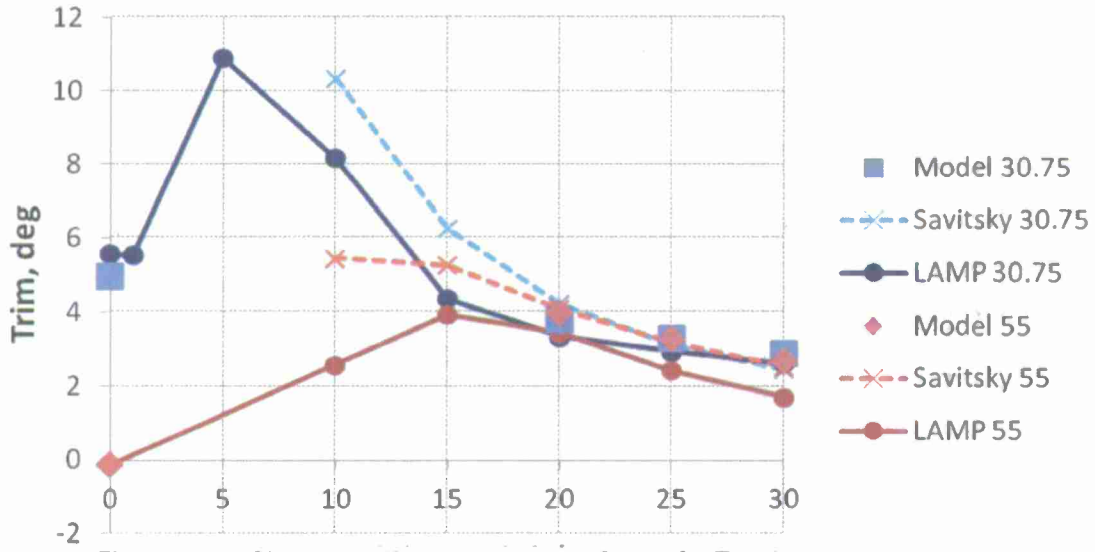

Figure 46. USNA Model Trim Angle versus Speed for Two Displacements.

CONCLUSIONS

A recent effort to assess the current ability of NFA and LAMP to predict the hydrodynamic forces and moments of a deep-V planing craft and how well they model the complex multiphase flows associated with high Froude number flows. To investigate the performance, data was utilized from three experiments: 1. a 10 degree wedge drop experiment performed at NSWCCD, 2. the classic planing boat work performed by Fridsma, and 3. a forced roll planing boat test performed at USNA. This detailed validation effort was composed of three parts.

For the wedge drop experiment, results show that NFA accurately predicted pressure time histories during the slamming event, for two different drop heights. LAMP predicted impact pressures using four different methods. All experimentally measured values were below the values predicted using the "Added Mass" method, and some were below the "Rich Lewis" method as well.

In the comparison to the Fridsma experiments, results show good agreement between NFA and the experimentally measured values of rise at CG, trim and resistance, as well as values calculated using Savitsky's parametric equations. Comparisons of the experimental data with the LAMP predictions show that LAMP tends to overpredict heave, but the trim comparison is good and is within 1 degree of the experimental measurements. Additional comparisons of LAMP RAOs with experimental RAOs were presented.

Comparisons to underwater photographs from the USNA forced roll experiment illustrated NFA's ability to model the formation of the spray sheet and the free surface turbulence associated with planing boat hydrodynamics. Generally, the LAMP predictions compare well with the experimental measurements for calm water heave and trim. For the heavy displacement, the LAMP trim prediction is low by about 1 degree, but the heave prediction matches the data well. Overall these three studies demonstrate the current capabilities of NFA and LAMP in predicting the hydrodynamics of a deep-V planing hull.

REFERENCES

[1] Fridsma, G. (1969), "A Systematic Study of the Rough-Water Performance of Planing Boats," *Davidson Laboratory Report*, Stevens Institute of Technology, Hoboken, New Jersey.

[2] Savitsky, D. (1964), "Hydrodynamic Design of Planing Hulls," *Marine Technology*, pp 71-95.

[3] Codega, L. and Lewis, J., (1987), "A Case Study of Dynamic Instability in a Planing Hull", *Marine Technology*, Vol. 24, No. 2, April, pp. 143-163.

[4] Blount, D. L. and Codega, L. T., (1992), "Dynamic Stability of Planing Boats", *Marine Technology*, Vol. 29, No. 1, Jan, pp. 40-12.

[5] Katayama, T., Fujimoto, M., and Ikeda, Y., (2007), "A Study on Transverse Stability Loss of Planing Craft at Super High Forward Speed", *International Journal of Fluid Mechanics Research*, Vol. 54, pp. 365-377

[6] Troesch, A.W., (1992), "On the Hydrodynamics of Vertically Oscillating Planing Hulls," *Journal of Research*, Vol. 36, No. 4, December, pp. 317-331.

[7] Troesch, A.W. and Falzarano, J. M., (1993) "Modern Nonlinear Dynamical Analysis of Vertical Plane Motion of Planing Hulls", *Journal of Research*, Vol. 37, No. 3, pp. 189-1991.

[8] Lewandowski, E. M., (1997), "Transverse Dynamic Stability of Planing Craft", *Marine Technology*, Vol. 34, No. 2, April, pp. 109-118.

[9] Broglia, R. and Iafrati, A., (2010), "Hydrodynamics of Planing Hulls in Asymmetric Conditions," *Proceedings of the 28th Symposium on Naval Hydrodynamics*, Pasadena, CA, September 12-17.

[10] Fu, T.C., Akers, R., O'Shea, T., Brucker, K., Dommermuth, D.G., & Lee, E., (2011), "Measurements and Computational Predictions of a Deep-V Monohull Planing Hull," *ITTC Coast Sea Trials*, Honolulu, HI, Sept 26-19.

[11] Fu, T.C., Ratcliffe, T., O'Shea, T., Brucker, K., Graham, R., Wyatt, D., & Dommermuth, D., (2010), "A Comparison of Experimental Measurements & Computational Predictions of a Deep-V Planing Hull," *Proceedings of the 28th Symposium on Naval Hydrodynamics*, Pasadena, CA, September 12-17.

[12] Jiang, M., Lien, V., Lesar, D.E., Engle, A., & Lewis, R., (2012), "A Validation of Various Codes Using Hydrodynamic Wedge Impact Data," *1st ITTC Coast Sea Trials Conference*, Rio de Janeiro, Brazil, July 1-6.

[13] O'Shea, T. T., Brucker, K. A., Dommermuth, D. G. & Wyatt, D. C., (2008), "A Numerical Formulation for Simulating Free-surface Hydrodynamics," *Proceedings of the 27th Symposium on Naval Hydrodynamics*, Seoul, Korea.

[14] Rottman, J. W., Brucker, K. A., Dommermuth, D. G. & Broutman, D., (2010), "Parameterization of the Internal Wave Field Generated by a Submarine and its Turbulent Wake

in a Uniformly Stratified Fluid," *Proceedings of the 28th Symp. on Naval Hydrodynamics.*, Pasadena, CA, USA.

[15] Dommermuth, D. G., O'Shea, T. T., Wyatt, D. C., Ratcliffe, T., Weymouth, G. D., Hendrikson, K. L., Yue, D. K., Sussman, M., Adams, P. & Valenciano, M., (2007), "An Application Of Cartesian-Grid And Volume-Of-Fluid Methods To Numerical Ship Hydrodynamics," *Proc. of the 9th Int. Conf. on Numerical Ship Hydrodynamics*, Ann Arbor, MI.

[16] Brucker, K. A., O'Shea, T. T. & Dommermuth, D. G., (2010), "Numerical Simulations of Breaking Waves – Weak Spilling to Strong Plunging," *Proc. of the 28th Sym. on Naval Hydrodynamics*, Pasadena, CA, Sept. 12-17.

[17] Heggelund, S.E., Haslum, H.A., Nilsen, J.A. and Zhao, R. (1998) "Slam2D Version 2.0 – User's Manual," MARINTEK REPORT, #603731.00.01.

[18] Bertram, V. (2002) "Practical Ship Hydrodynamics," pp. 138-141.

[19] Band, E.G.U. (1969), "Study of Bow Impact Loads for 100-ton Surface Effect Ship," Payne Division of Wyle Labs, Working Paper No 18008-2, Aerojet General Corporation.

[20] Lewis, Richard R., "Peak Structural Responses and Pressures from Hydrodynamic Impact Tests of Weges with Structural Grillage Inserts," CARDEROCKDIV-U-SSM-65-95/34, May 1995.

[21] Wagner, Herbert, "The Phenomena of Impact and Planing on Water," NACA Translation 1366, August 1932.

[22] Lesar, D.E., Jiang, M., Lien, V., Engle, A. & Lewis, R. (2012) "Validation of Numerical Analysis Codes for Hydrodynamic Impact Simulation Using Rigid Wedge Drop Test Data," Draft *NSWCCD Technical Report*.

[23] Bruno, M. S., (1993), "Davidson Laboratory and the Experimental Towing Tank: The History of Towing Tank Research at Stevens", SNAME, New York Metropolitan Section, (book).

[24] Judge, C.Q., (2010), "Frequency Dependence of Hydrodynamic Coefficients in Roll", Proceedings of the 29th American Towing Tank Conference, Annapolis, MD, 2010, pp. 285-290.

APPENDIX A: HEAVE AND PITCH RESPONSE AMPLITUDE OPERATOR LAMP COMPARISON FOR THE PRISMATIC HULL FORMS

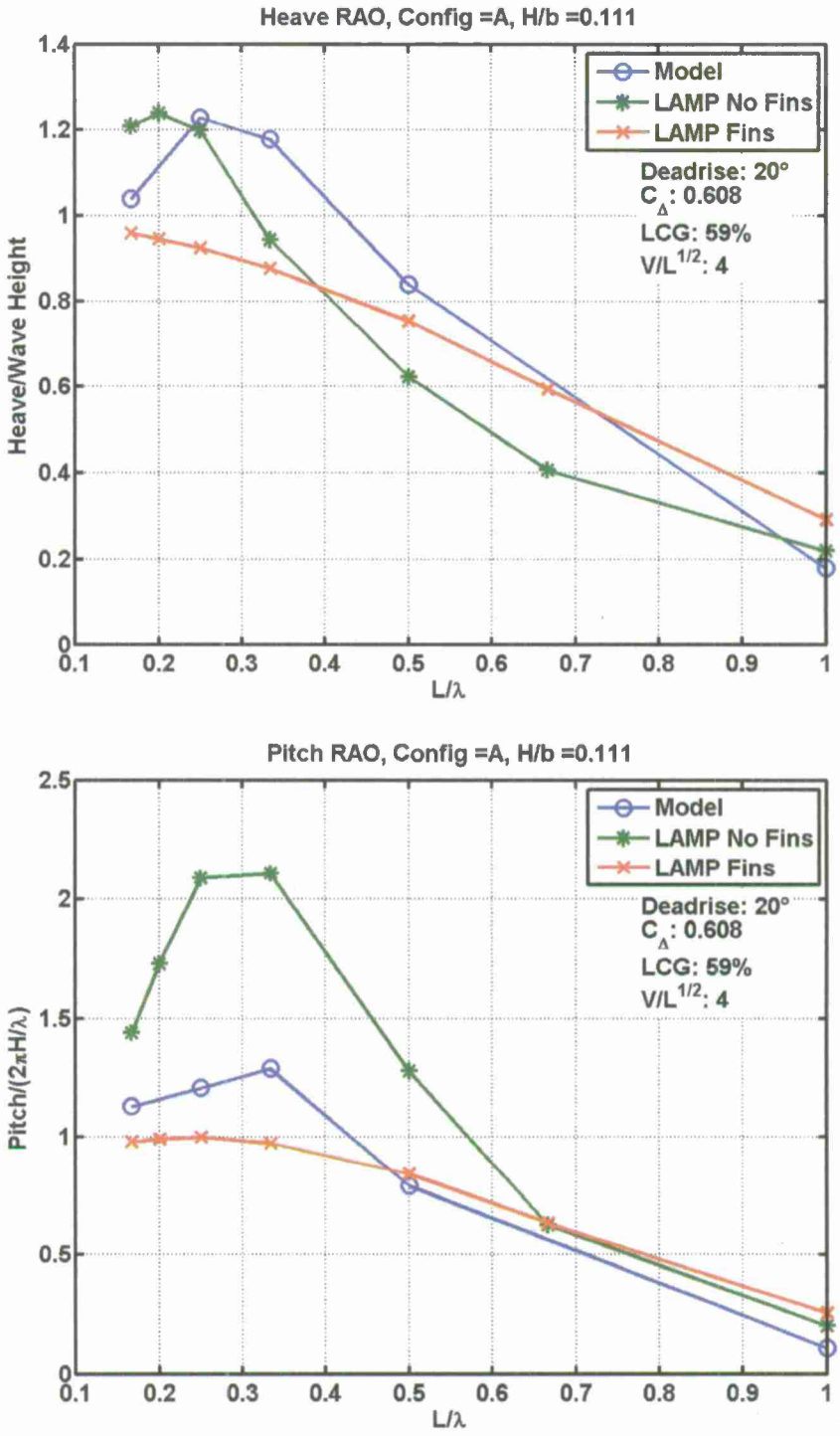

Figure A-1: Heave and Pitch RAO Comparison for Configuration A.

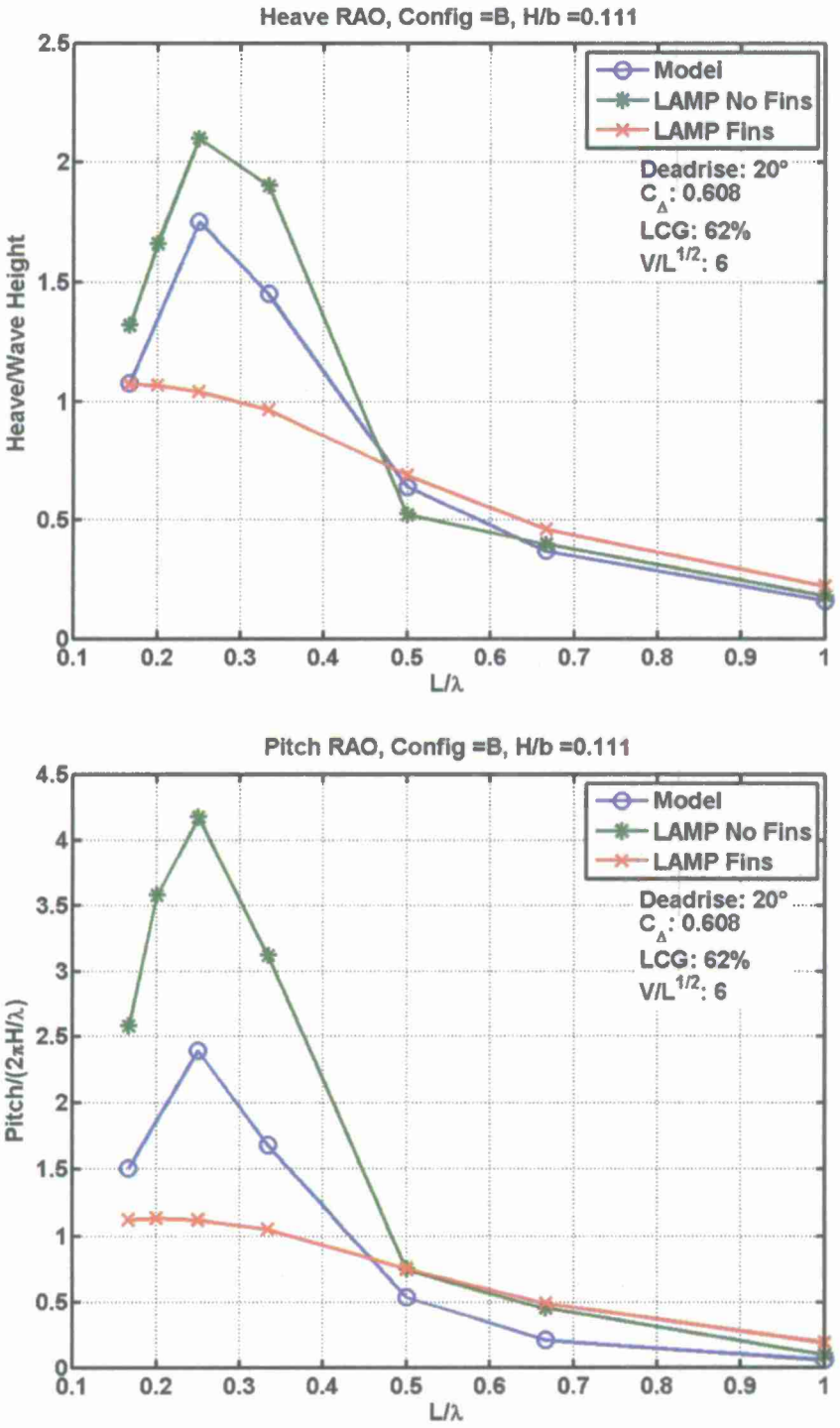

Figure A-2: Heave and Pitch RAO Comparison for Configuration B.

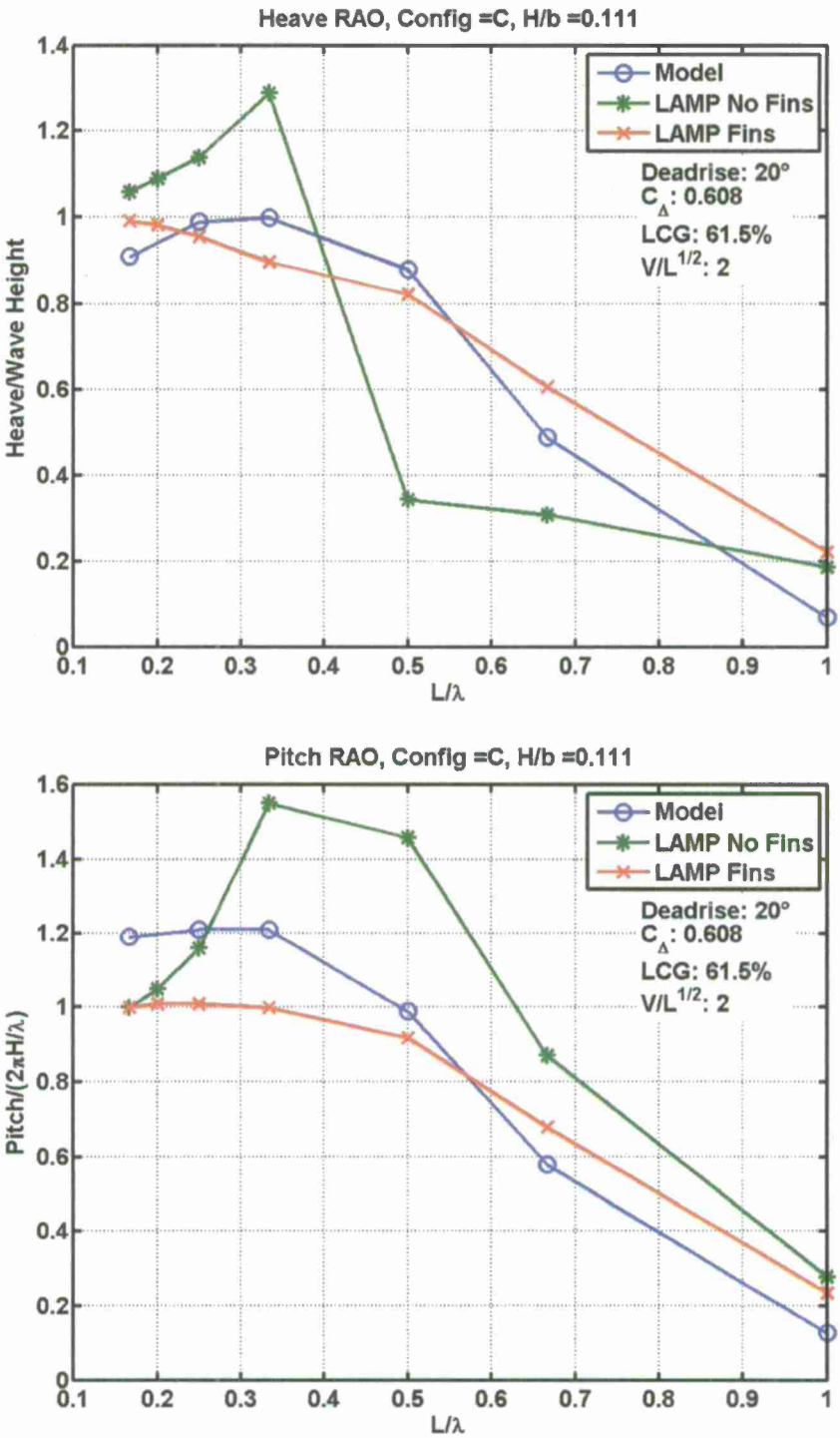

Figure A-3: Heave and Pitch RAO Comparison for Configuration C.

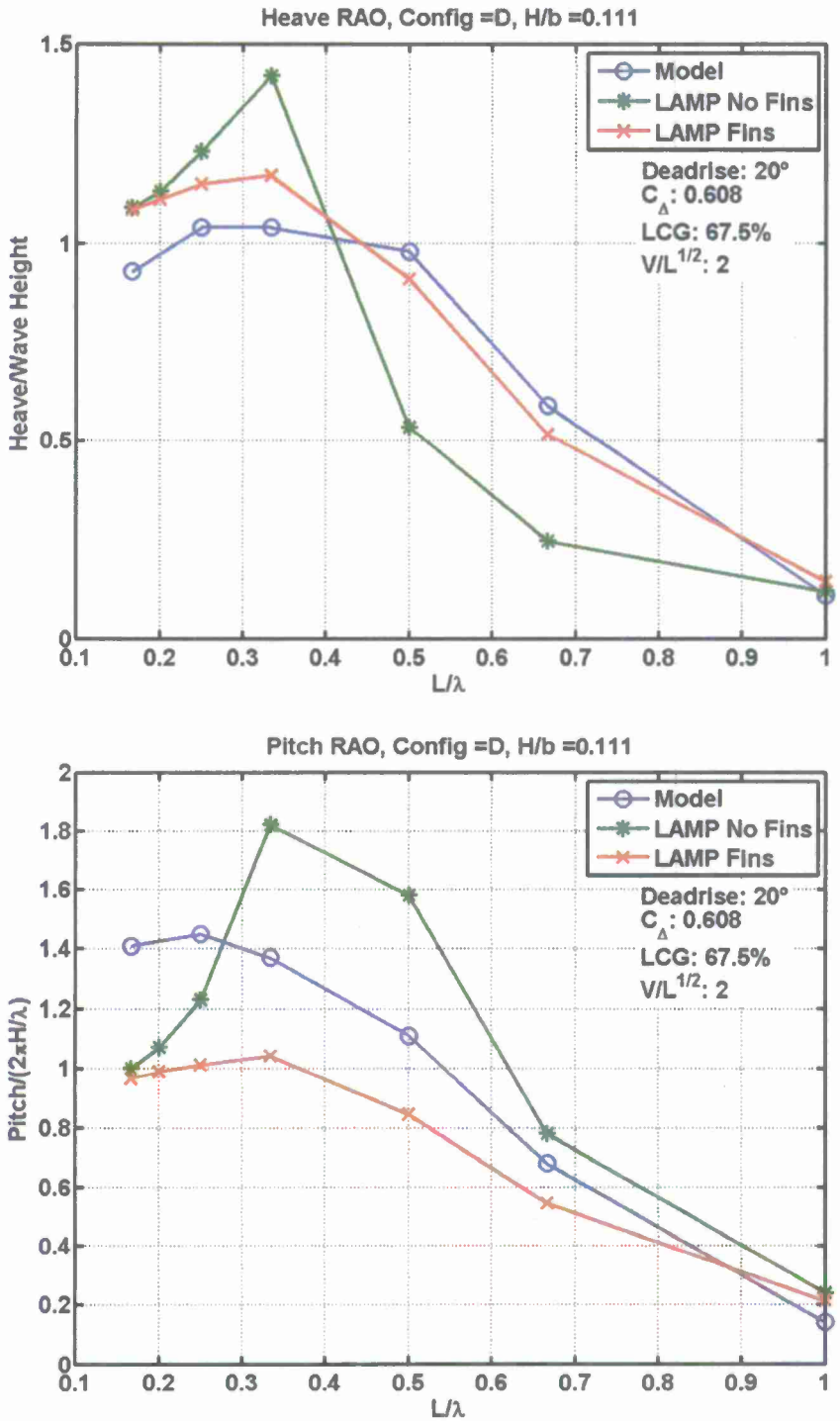

Figure A-4: Heave and Pitch RAO Comparison for Configuration D.

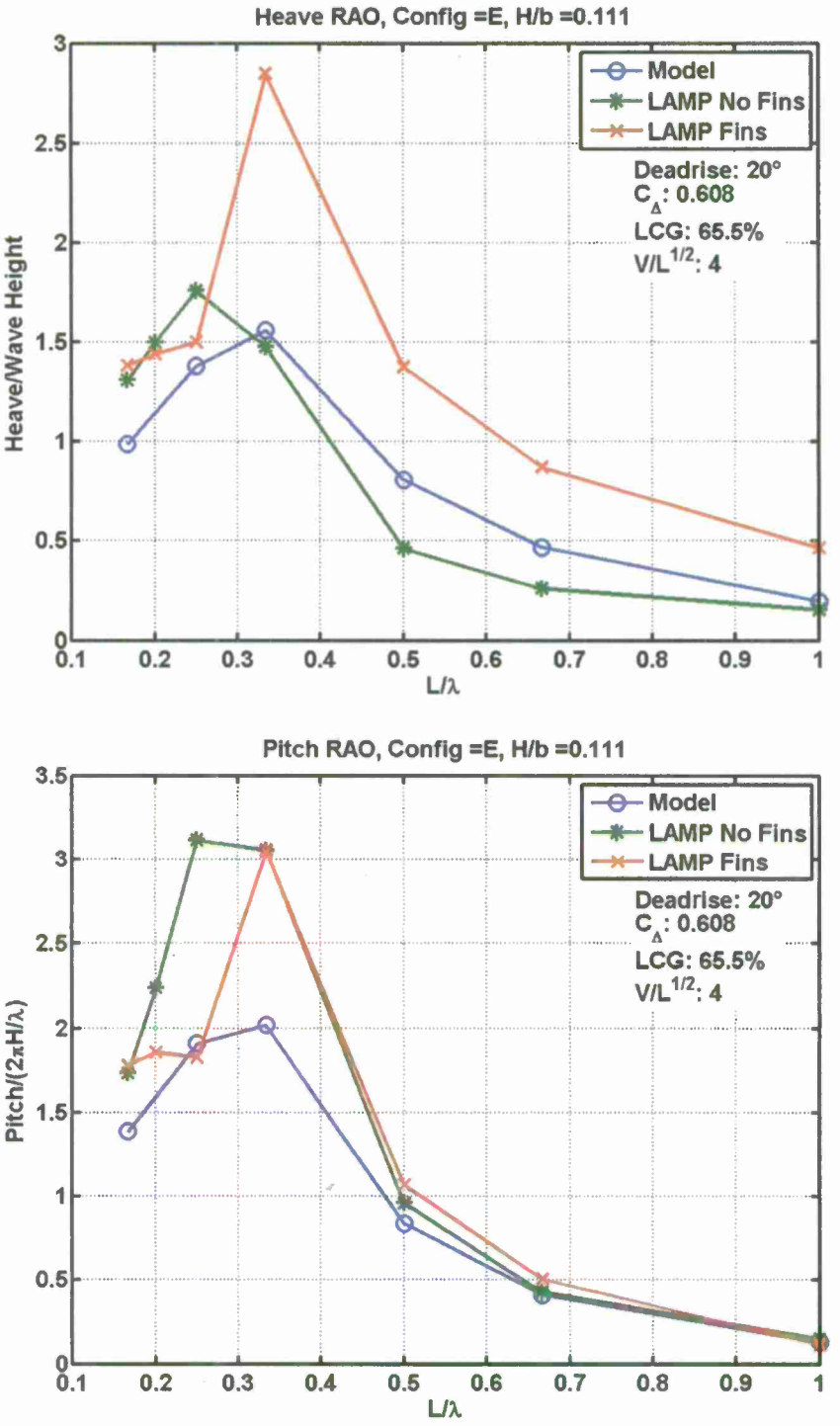

Figure A-5: Heave and Pitch RAO Comparison for Configuration E.

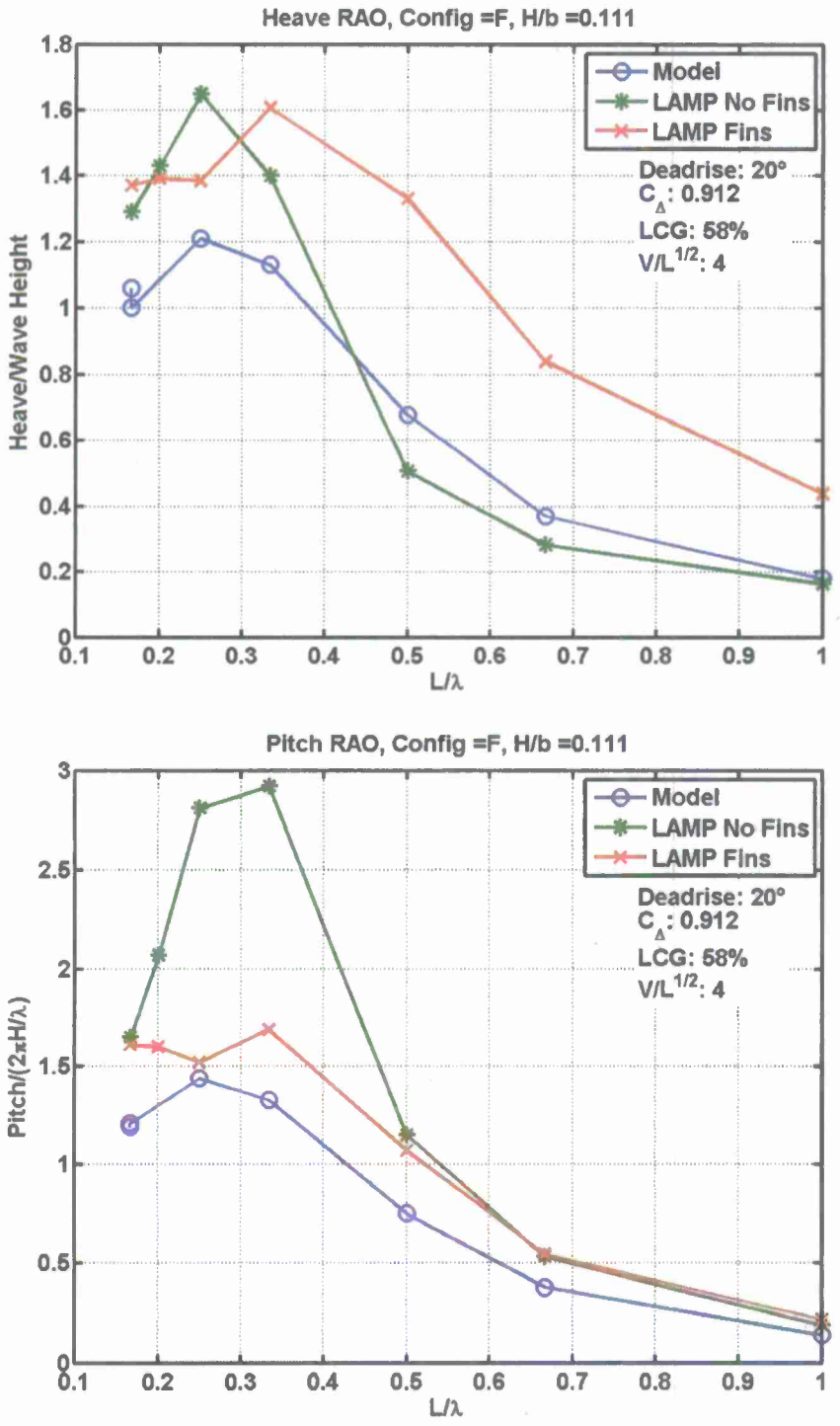

Figure A-6: Heave and Pitch RAO Comparison for Configuration F.

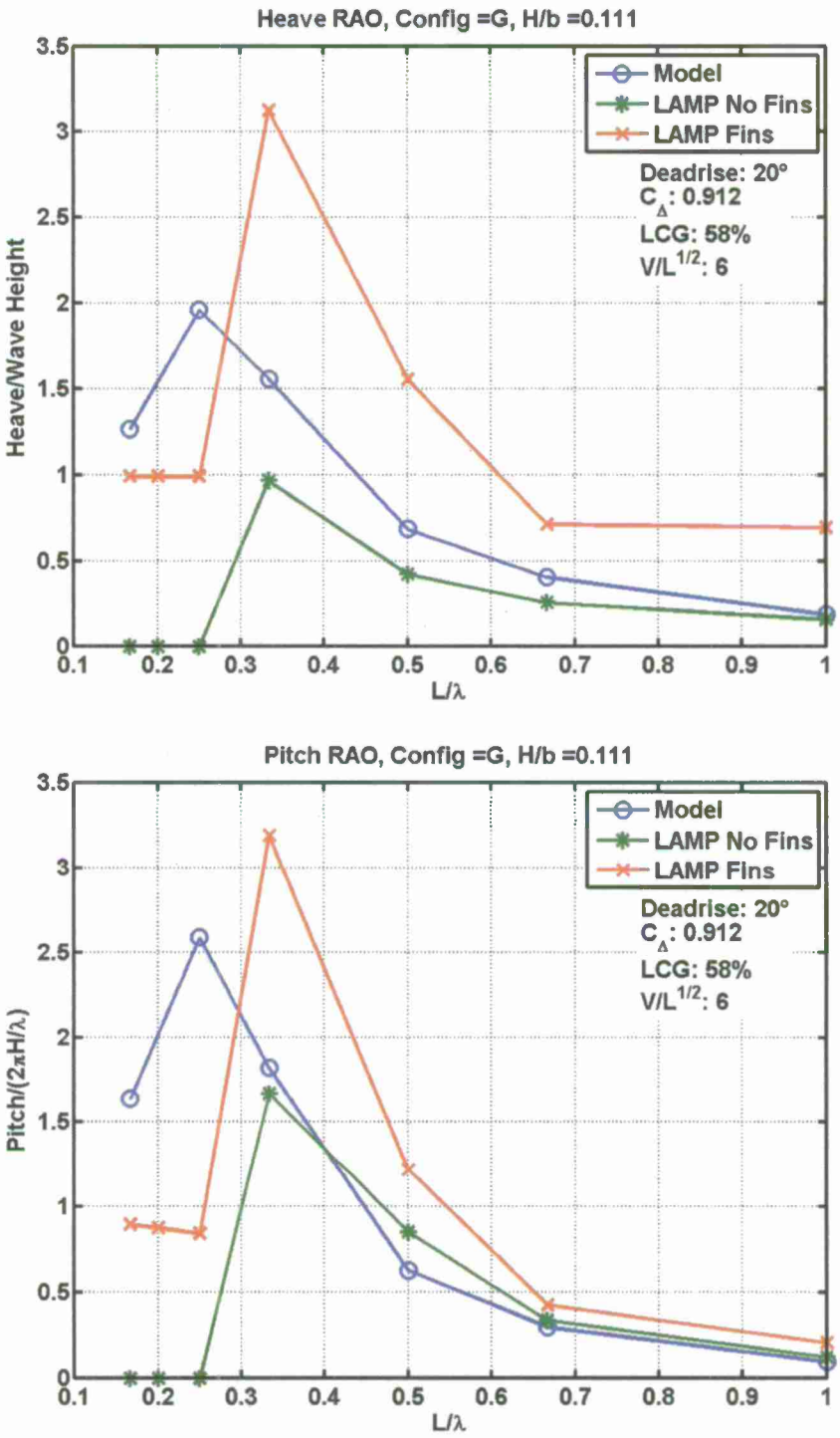

Figure A-7: Heave and Pitch RAO Comparison for Configuration G.

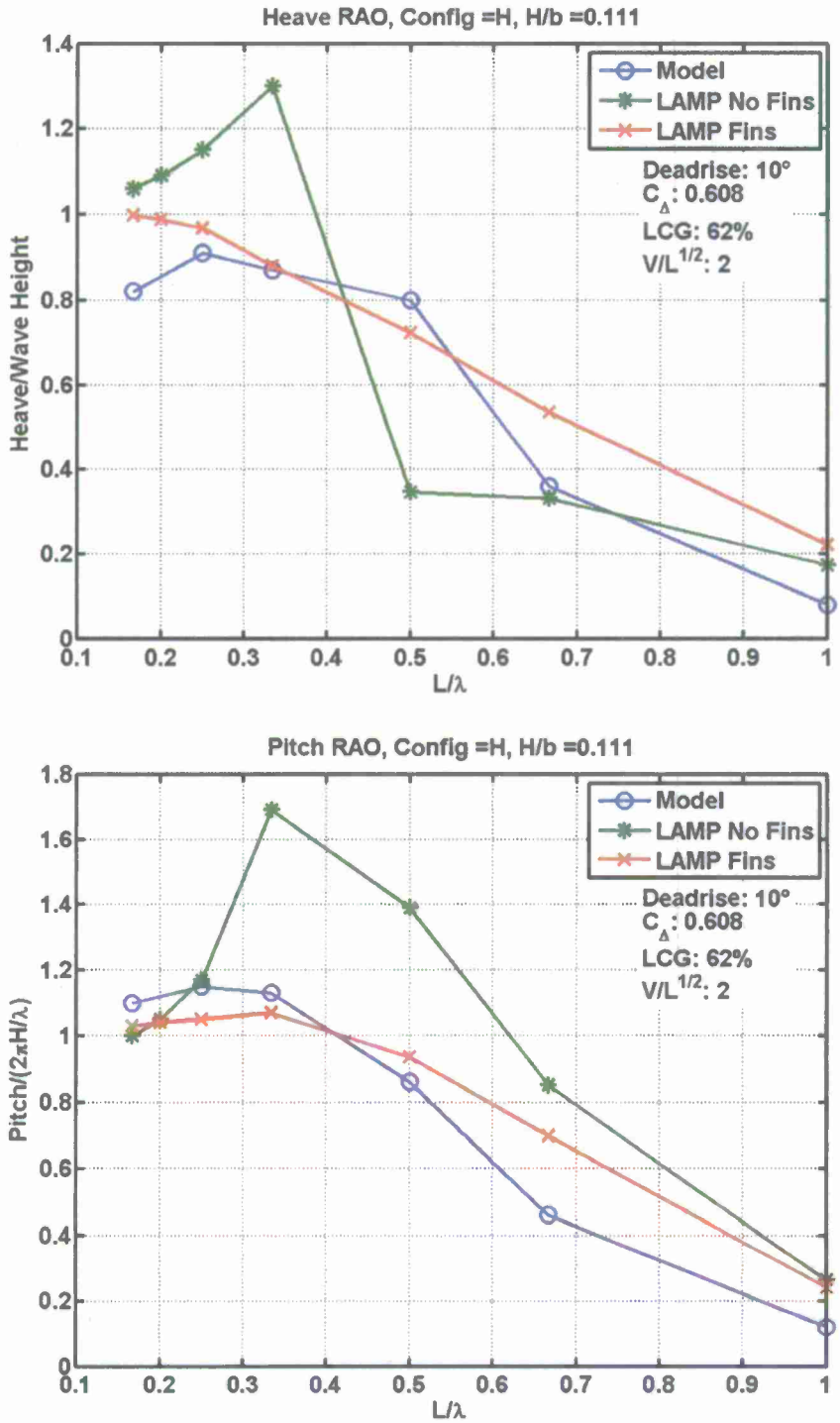

Figure A-8: Heave and Pitch RAO Comparison for Configuration H.

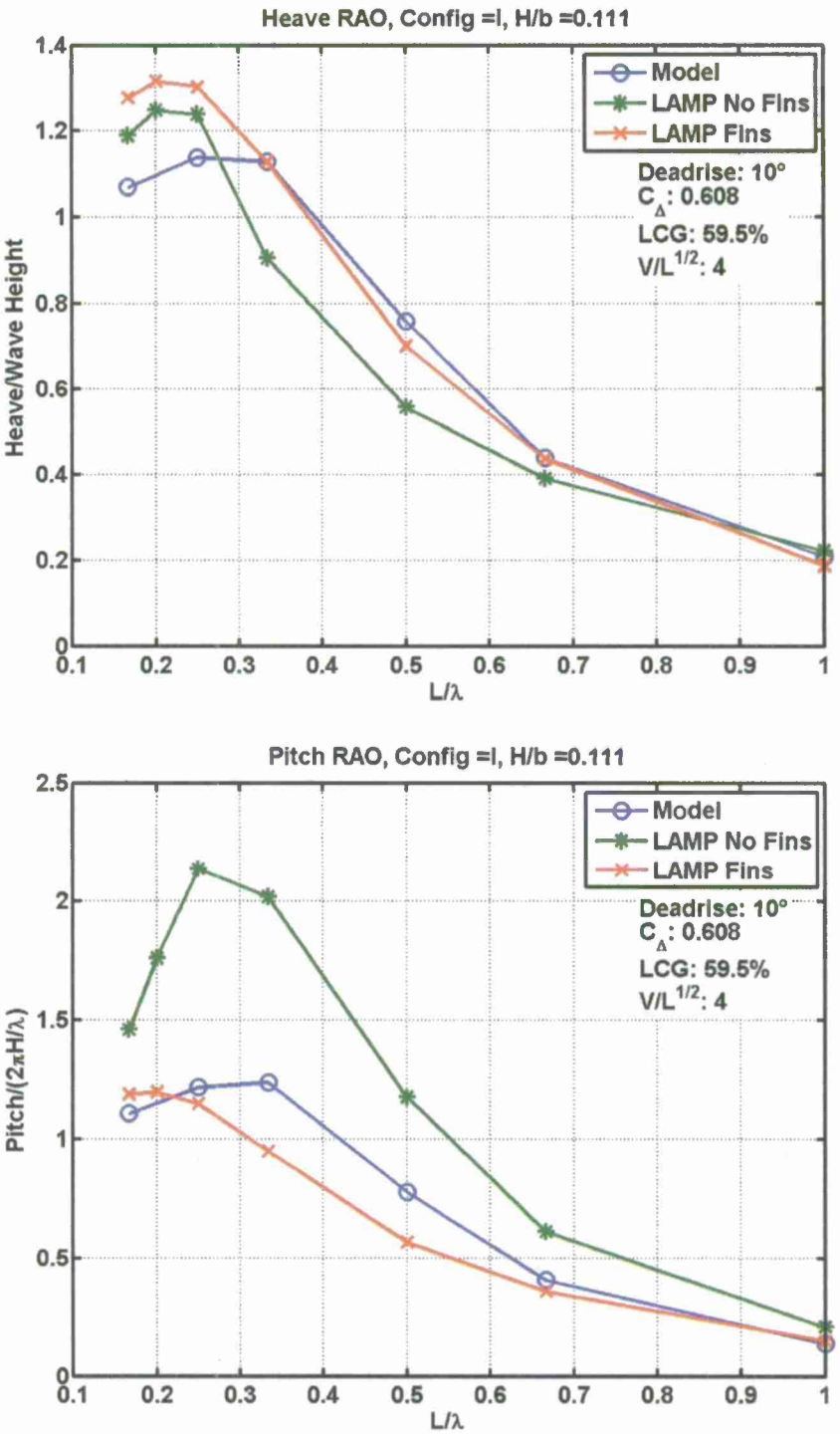

Figure A-9: Heave and Pitch RAO Comparison for Configuration I.

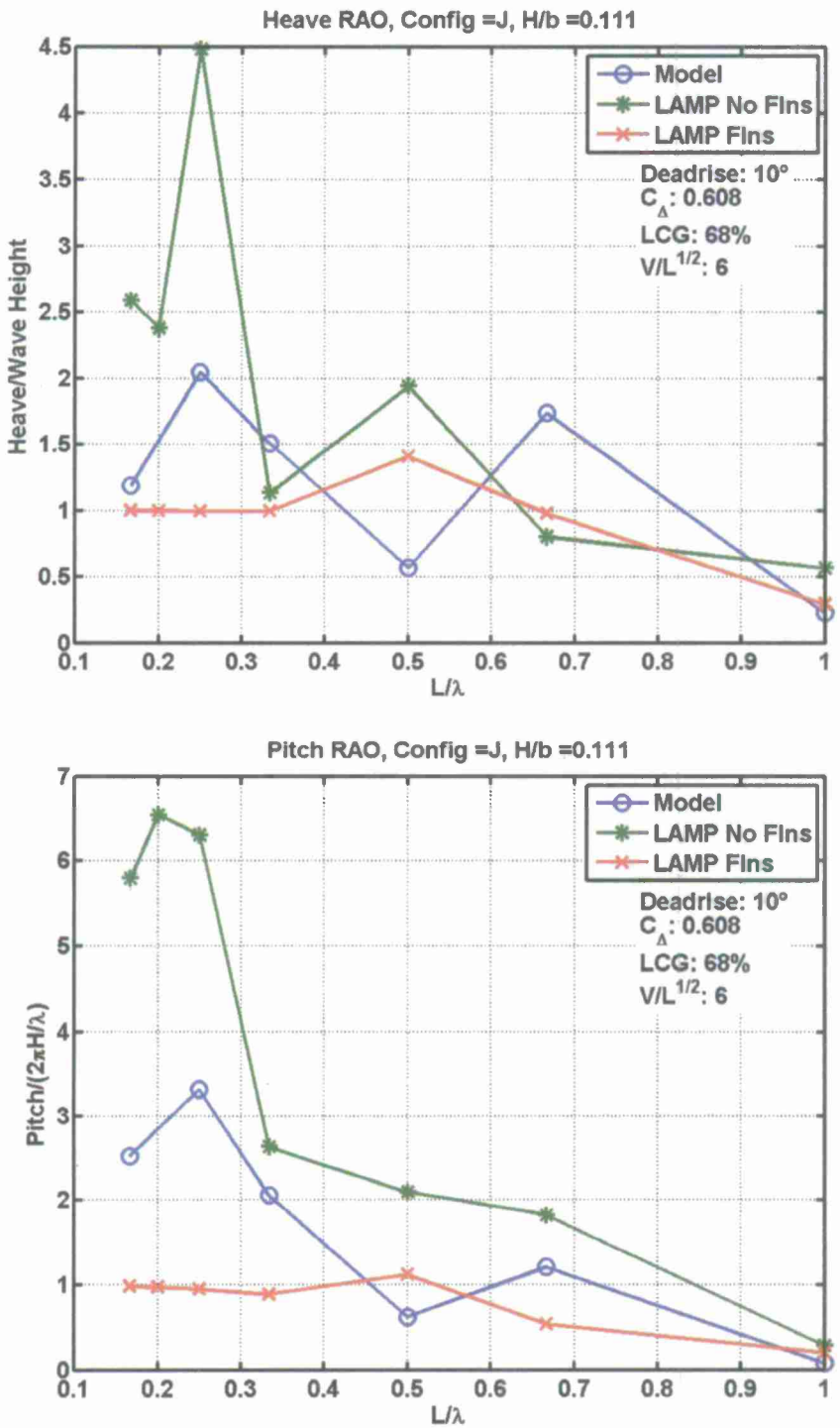

Figure A-10: Heave and Pitch RAO Comparison for Configuration J.

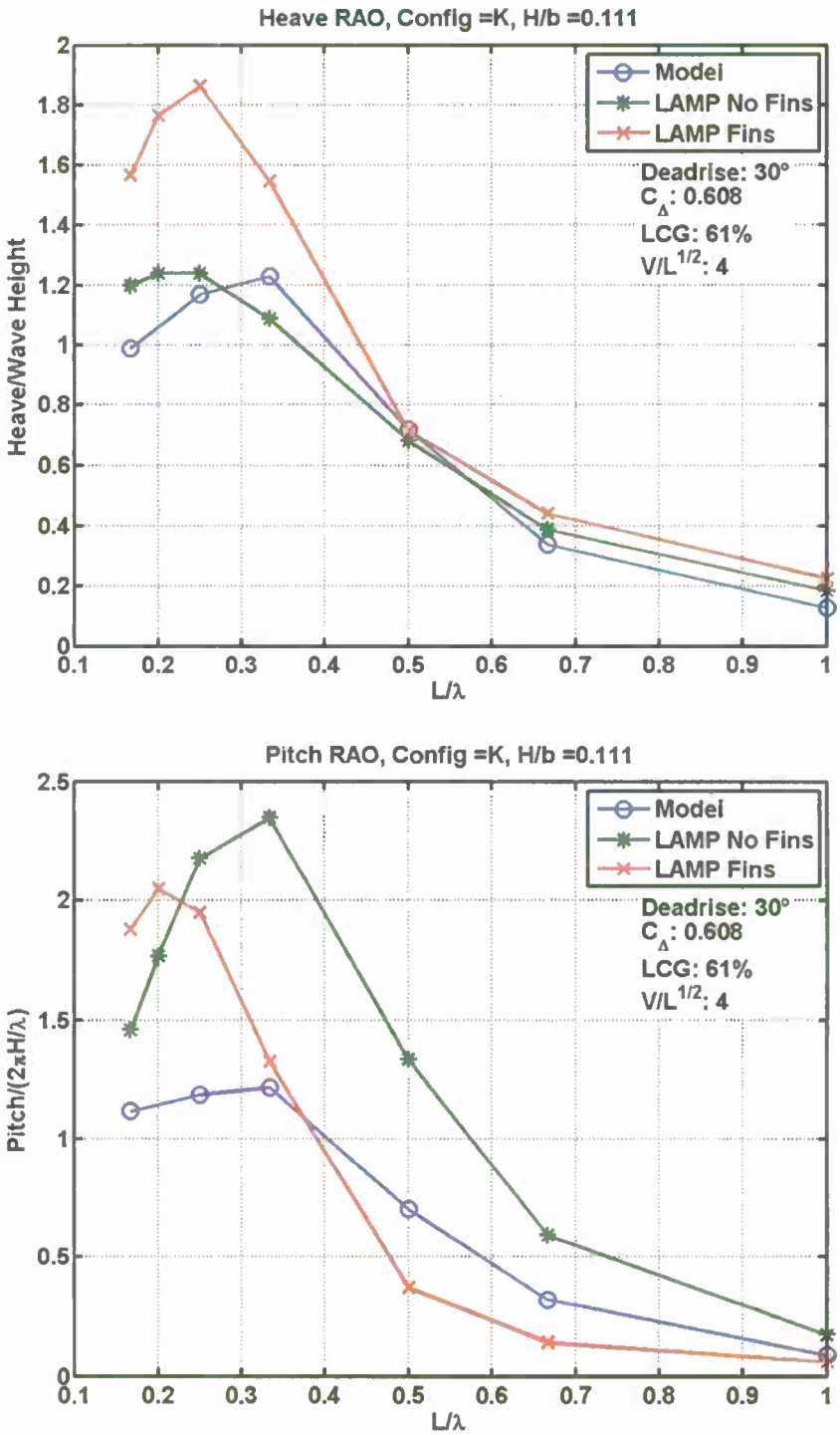

Figure A-11: Heave and Pitch RAO Comparison for Configuration K.

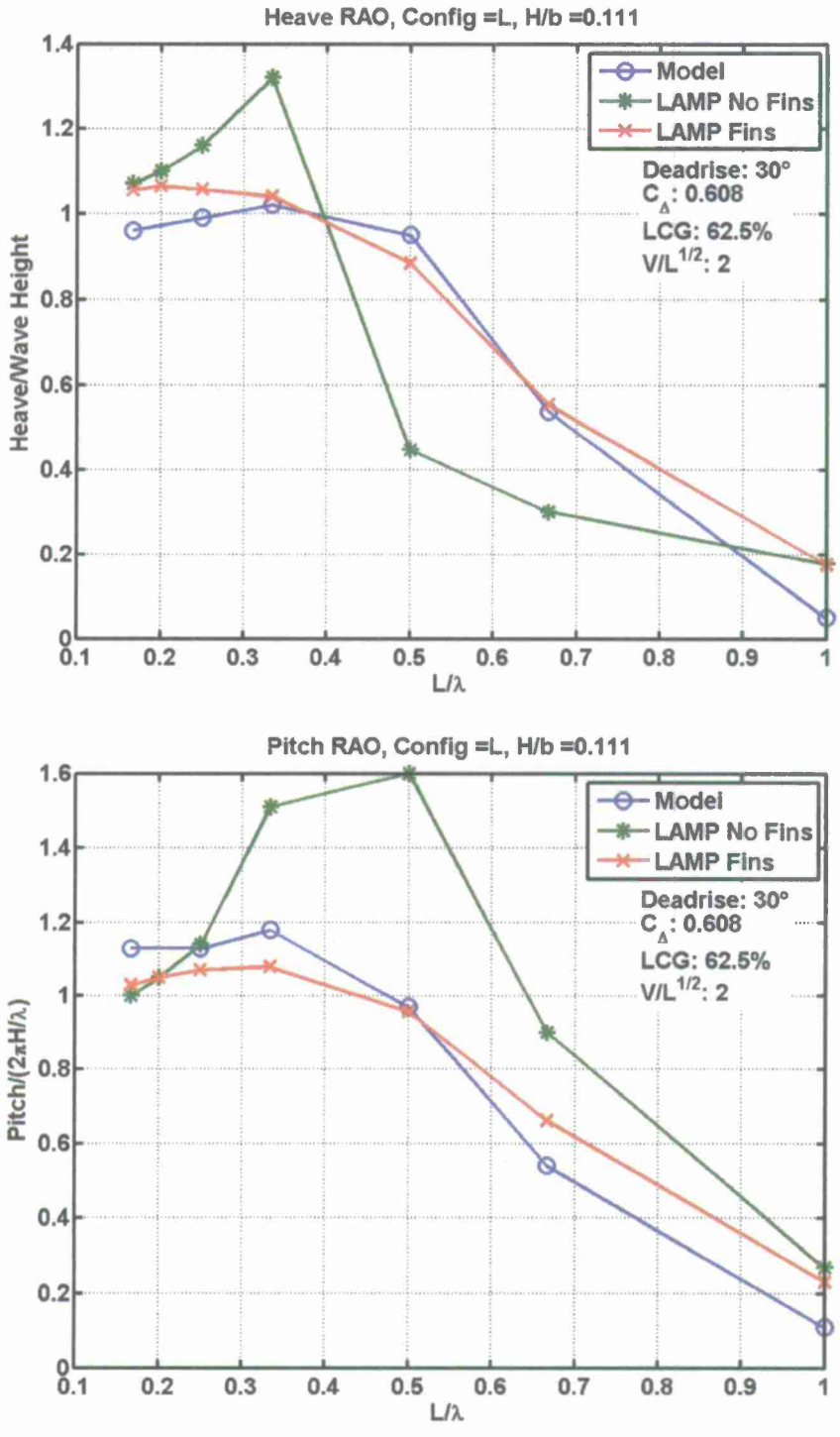

Figure A-12: Heave and Pitch RAO Comparison for Configuration L.

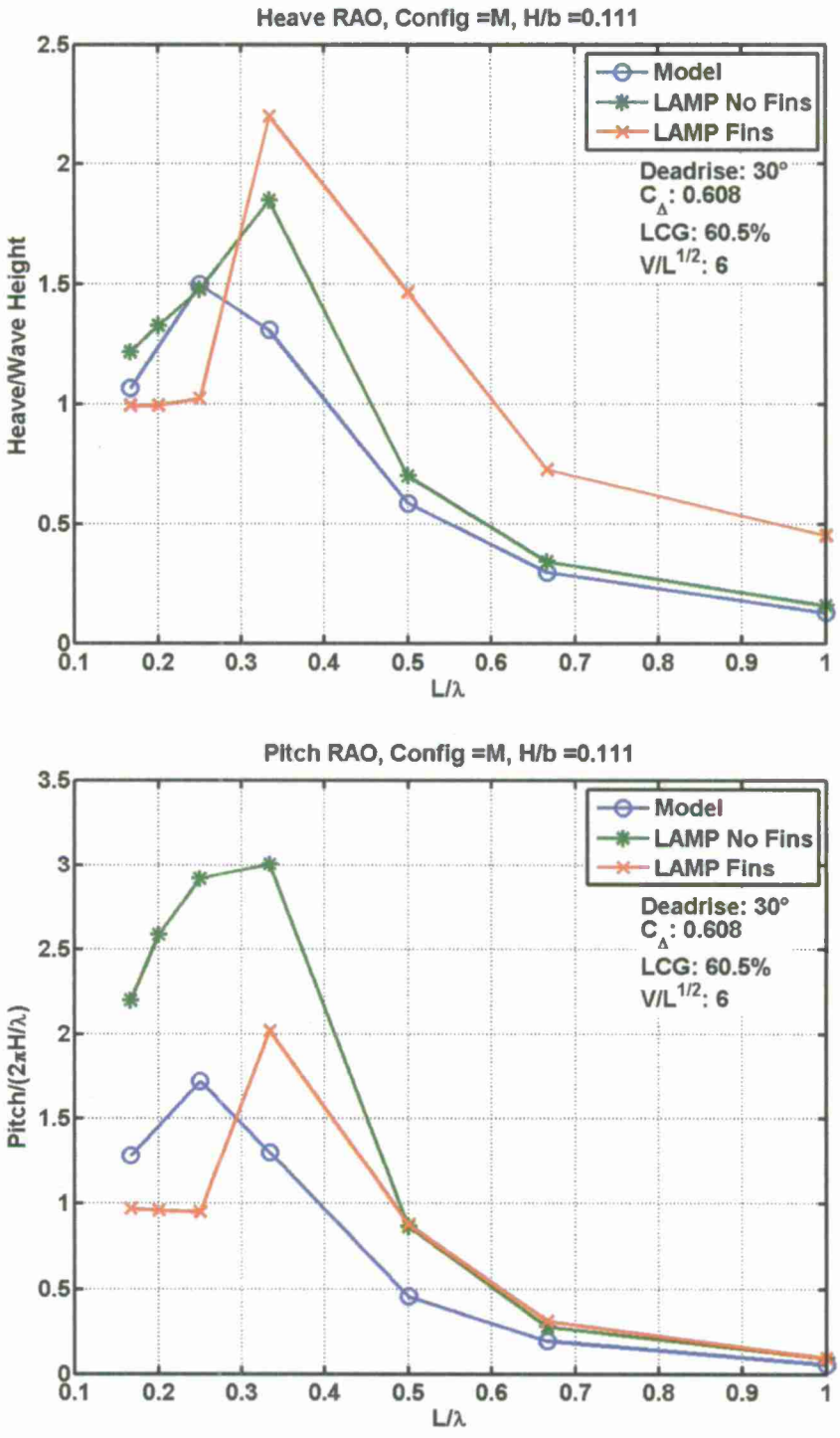

Figure A-13: Heave and Pitch RAO Comparison for Configuration M.

DISTRIBUTION LIST

Copies		Name
NAVSEA		
1		DTIC
Division Distribution		
1	3452	Library (pdf only)
1	5050	Thomas Fu (pdf only)
4	5830	Anne Fullerton, Craig Merrill, (pdf only), Files (2)
1	5510	Christopher Bassler (pdf only)
1	654	Allen Engle (pdf only)
ONR		
1		Robert Brizzolara
SAIC		
4		Don Wyatt, Tom O'Shea, Kyle Brucker, Doug Dommermuth (pdf only)